AFIT/GEP/ENP/92D-07

ELECTRONIC-TO-VIBRATIONAL (E⇨V) ENERGY TRANSFER FROM Br* TO CO_2 & (E⇨V) LASER FEASIBILITY STUDIES

THESIS

Steven M. Katapski

Captain, USAF

AFIT/GEP/ENP/92D-07

AFIT/GEP/ENP/92D-07

ELECTRONIC-TO-VIBRATIONAL (E⇨V) ENERGY TRANSFER FROM Br* TO CO_2 & (E⇨V) LASER FEASIBILITY STUDIES

THESIS

Presented to the Faculty of the School of Engineering

of the Air Force Institute of Technology

Air University

In Partial Fulfillment of the

Requirements for the Degree of

Master of Science in Engineering Physics

Steven M. Katapski, B.S.

Captain, USAF

October 1992

Preface

This research continues investigations in the field of electronic-to-vibrational (E ⇨ V) energy transfer from gas-phase Br($4^2P_{½}$) atoms to CO_2 and subsequent lasing of the excited CO_2 species at 4.3 μm. An apparatus was designed and constructed to photo-dissociate molecular bromine, accommodate energy transfer to the CO_2, and permit lasing of the desired transition ([101] - [100]). The work, though at times frustrating, was quite gratifying in that I was able to reproduce important data, and gain at least a summary understanding of gas kinetics along the way.

I wish to thank Major Glen Perram, my advisor for all his advice and keen insight. His patience with my all my theory questions and complaints about hardware was extraordinary. Dr. Won Roh also provided much technical advice and support when needed. My thanks also to my lab partner, Capt Ray Johnson, a doctoral student working on related research. Ray provided much initial hand-holding as I struggled to understand the complexities of the lab environment and the interpersonal relationships among the Engineering Physics Dept staff. His assistance with theory development and data analysis is also greatly appreciated. Lastly, I owe a great debt to my children, Ryan and Lindsey. Though they live several thousand miles from Ohio, they always provided the kind words that only innocent young children can to let me know that no matter how crazy things were getting with my research, that their love and prayers were with me.

Steven M. Katapski

Table of Contents

Table of Contents (Cont.)

List of Figures

Figure

List Of Tables

Table

Abstract

The energy transfer mechanism from photo-excited bromine atoms ($Br(^2P_{1/2})$) to CO_2 is investigated in a pulsed fluorescence experiment. An excimer-pumped pulsed dye laser operating at 480 nm is used to photolyze molecular bromine, resulting in the creation of one excited state bromine atom, $Br(^2P_{1/2})$, and one ground state atom, $Br(^2P_{3/2})$. The electronically-excited bromine atoms (referred to as Br*) collide with and excite vibrational modes in the ground electronic state of CO_2. Measurements are made of the Br* lifetimes and associated quenching processes, and the electronic-to-vibrational (E⇨V) energy transfer rate from Br* to CO_2. The feasibility of subsequent stimulated emission from the CO_2 on the [101] - [100] (4.3 μm) transition is studied, and attempts are made to achieve lasing. Limitations of the experimental apparatus prevented achieving stimulated emission on the 4.3 μm transition. Recommendations are made for improvements in the analysis and apparatus for further research.

ELECTRONIC-TO-VIBRATIONAL (E⇨V) ENERGY TRANSFER FROM Br* TO CO_2 & (E⇨V) LASER FEASIBILITY STUDIES

I. Introduction

Overview

An Air Force requirement exists to develop kilowatt-class lasers operating at infrared wavelengths for anticipated electro-optic countermeasure missions. To that end, several studies have been pursued to identify potential candidate technologies. One concept involves utilizing gas-phase molecular lasers. Several researchers have investigated using energy transfer from photo-excited bromine atoms to collisionally excite near-resonant vibrational modes of CO_2, resulting in stimulated emission at 4.3, 10.6, and 14.1 μm (11:1051).

This thesis expands the current data base on electronic-to-vibrational (E⇨V) energy transfer from excited state bromine atoms ($Br(^2P_{1/2})$) to CO_2. An experiment was designed and performed and the results of that research are presented here.

Background

The $Br(^2P_{1/2})$ electronically excited state of the bromine atom resides at 3685.0 cm^{-1} above the ground state ($Br(^2P_{3/2})$). The excited state is achieved as a result of spin-orbit coupling. The electric dipole transition to the ground state is strongly forbidden and hence, the lifetime of the excited state is long--approximately 1.1 seconds (7:160). Detection of this spontaneous emission can be achieved with side fluorescence detection techniques as will be described later. Electronic excitation is achieved by laser photolysis techniques. Excited bromine atoms in the $^2P_{1/2}$ state have been shown to readily transfer

their energy to near-resonant molecular species via the electronic-to-vibrational (E⇨V) energy transfer process. CO_2 has been shown to be a viable recipient due to its near-resonant vibrational energy levels and favorable quenching rate on Br*. Vibrational modes are excited in the CO_2 molecule, and with the proper choice of cavity characteristics, stimulated emission on a variety of ro-vibrational transitions can be achieved. Specifically, interest lies in stimulating the [101] to [100] transition resulting in lasing action at 4.3 μm.

Problem Statement

Much interest lies in developing tunable high-power lasers in the 3-5 μm regime for various Air Force applications. The key to an effective weapon (or countermeasure, in this case) is resistance to countermeasures. This is achieved in a laser device by providing tunability of the output wavelength, so as to make defensing against the device more difficult. Molecular infrared lasers achieve this tuning capability by selecting individual ro-vibrational transitions using cavity characteristics (intracavity etalon, gratings, etc.). This thesis effort consists of designing, constructing and demonstrating the operation of a CO_2 laser operating at 4.3 μm using the E⇨V energy transfer process from excited Br atoms to populate the upper laser level.

Summary of Current Knowledge

The electronic-to-vibrational energy transfer process from excited bromine to various molecular species has been the subject of several investigations. Leone and Wodarczyk made the first direct measurements of the efficiency of the process, using HCl and HBr as the recipient species. Vibrational excitation ($v = 1$) was achieved in both species, resulting in 95% and 65% efficiencies, respectively (1:4454). Later Hariri and Wittig, using a variety of recipient molecular species, demonstrated energy transfer from $Br(^2P_{1/2})$

(hereinafter referred to as "Br*"). Rate coefficients for the quenching of Br* by CO_2 and the bromine parent molecule are obtained by examining the following reactions:

$$Br^* + Br_2 \rightarrow Br + Br_2 \quad (1.1)$$

$$Br^* + CO_2 \rightarrow Br + CO_2 \text{ (all states)} \quad (1.2)$$

Rates were determined by measuring both Br* and excited CO_2 fluorescence. Lifetimes of Br* and, in one case, the [001] state of CO_2 were determined using standard curve-fitting techniques applied to fluorescence data obtained using appropriate interference filters to isolate the 2.71 μm Br* transition, and the [001] - [000] transition in CO_2 (4.3 μm). A Stern-Volmer analysis was then performed to get the desired quenching rates. A measured E⇨V rate of $(6 \pm 0.1) \times 10^{-12}$ cm^3 $molecule^{-1}$ sec^{-1} was obtained, with the [101] state of CO_2 being identified as the major recipient of the transferred energy (1:4458). The quenching rate of CO_2 on Br* is related to the E⇨V rate, as a certain fraction (~40%) of the quenching collisions result in vibrational excitation. Additionally, a Br*-CO_2 laser was demonstrated with stimulated emission being achieved on the [001] - [100] band at 10.6 μm. A dye laser operating at 485 nm was used as the pump source to photolyze the Br_2 and produce Br*. An operating efficiency of nearly 15% was achieved (1:4460).

Peterson and Wittig conducted one of the earliest Br* - CO_2 laser demonstrations in 1975. In their experiment, the Br_2 was flash photolyzed with an input pulse energy of ~1000 J with a 2 μsec rise time and a 20 μsec FWHM. The photolysis flash was directed into the laser tube through a liquid dye medium (7-diethylamino 4-methyl coumarin) to convert UV photons from the flashlamp to visible wavelengths. Pump light was limited to the $330 \leq \lambda \leq 530$ nm region, which most effectively produces Br* (10:305). The authors speculated that the Br* energy was transferred to several near-resonant excited CO_2 states ([101], [021], etc.). However, it was not possible to determine precise states via

fluorescence techniques, as these states undergo rapid vibrational-to-vibrational (V⇨V) energy transfer to lower CO_2 states ([100], [001], and [010]). Stimulated emission was observed on P-branch transitions of the 10.6 μm band with a peak optical gain of 0.018 cm^{-1} being achieved. This maximum gain was achieved with total gas pressures of 16 torr (1:1 ratio of [Br_2] and [CO_2]) and flash lamp energies of 700 J (10:305).

Peterson and Wittig continued their work in the area of E⇨V lasers later that same year by concentrating on the Br* - CO_2 laser operating at several different wavelengths (4.3, 10.6 and 14.1 μm). Additional details from this work indicate that the cavity utilizes high-reflective gold-coated mirrors with a 0.5 mm hole in one mirror (R = 10 m) for output coupling. Suppression of individual transitions was achieved by introducing certain gas species into an intracavity absorption cell. The authors report achieving a maximum 10.4 μm laser pulse of 112 mJ about 10 μsec wide beginning 8 μsec after onset of photolysis. Pulse energy did not appear to be sensitive to gas mixtures (11:1052). Lasing was achieved at 4.3 μm when using gas mixtures more dilute in CO_2. In fact, lasing was detected on the 4.3 μm transition in CO_2 when investigating Br_2 - OCS gas mixtures *with CO_2 as an impurity*. The 4.3 μm transition occurred near 2304 cm^{-1} and was assigned to the P-branch of the [101] - [100] band. Transitions from the nearby [021] level were ruled out as the center frequency of the likely band ([021] - [020]) was too far from the observed frequency. The authors suggest that a more precise measurement of the 4.3 μm transition would confirm the assignment of the [101] - [100] band as the likely E⇨V pathway (11:1053). The strongest laser pulse achieved at 4.3 μm was ~ 0.1 mJ. The output pulse was generally 5 μsec wide, occurring some 10 - 15 μsec after the photolysis flash. Lasing was not observed at CO_2 pressures above 0.15 torr. Depopulation of the upper laser level via V⇨V energy transfer is suspected at higher pressures (11:1053).

The most recent attempt to demonstrate a Br* - laser system was undertaken by Pastel *et al.* in 1991. Unlike previous efforts, photolysis of the host species (in this case, IBr) was achieved using a frequency-doubled Nd:YAG pulsed laser operating at 532 nm. The pump source was directed into the cavity via a right angle prism at a small angle (~ 0.6°) with respect to the laser cavity axis. A prism was inserted at the far end of the cavity as well to direct the pump beam out of the cell, thus avoiding damage to the infrared optics. A 75% - reflective flat output mirror at one end served to output couple the CO_2 laser energy. Pump pulse energies were typically < 250 mJ with a FWHM pulse width of 5 nsec. Optimum output pulse energies of 0.1 mJ were obtained at 0.7 torr of CO_2 and 3 torr of IBr. FWHM of the 4.3 μm pulse was approximately 200 nsec, occurring some 350 nsec after the pump pulse. At 3 torr of IBr, lasing was not observed at CO_2 pressures above 1 torr (8:569). Recent personal communication with Pastel indicates that a minimum of ~12 mJ of pump pulse energy was necessary to achieve lasing action.

Scope

The objective of this thesis research will be to concentrate on replicating previous work on Br* - CO_2 lasers operating at 4.3 μm. An excimer-pumped dye laser will be used as a pump source to photolyze molecular bromine, resulting in E⇨V transfer to CO_2. Output pulse energies at 4.3 μm will be detected for a variety of gas mixes in an attempt to characterize system performance.

Approach

An experimental apparatus will be designed to accommodate the handling of bromine and CO_2 and an appropriate laser resonator constructed. Figure 1.1 shows the proposed experimental setup.

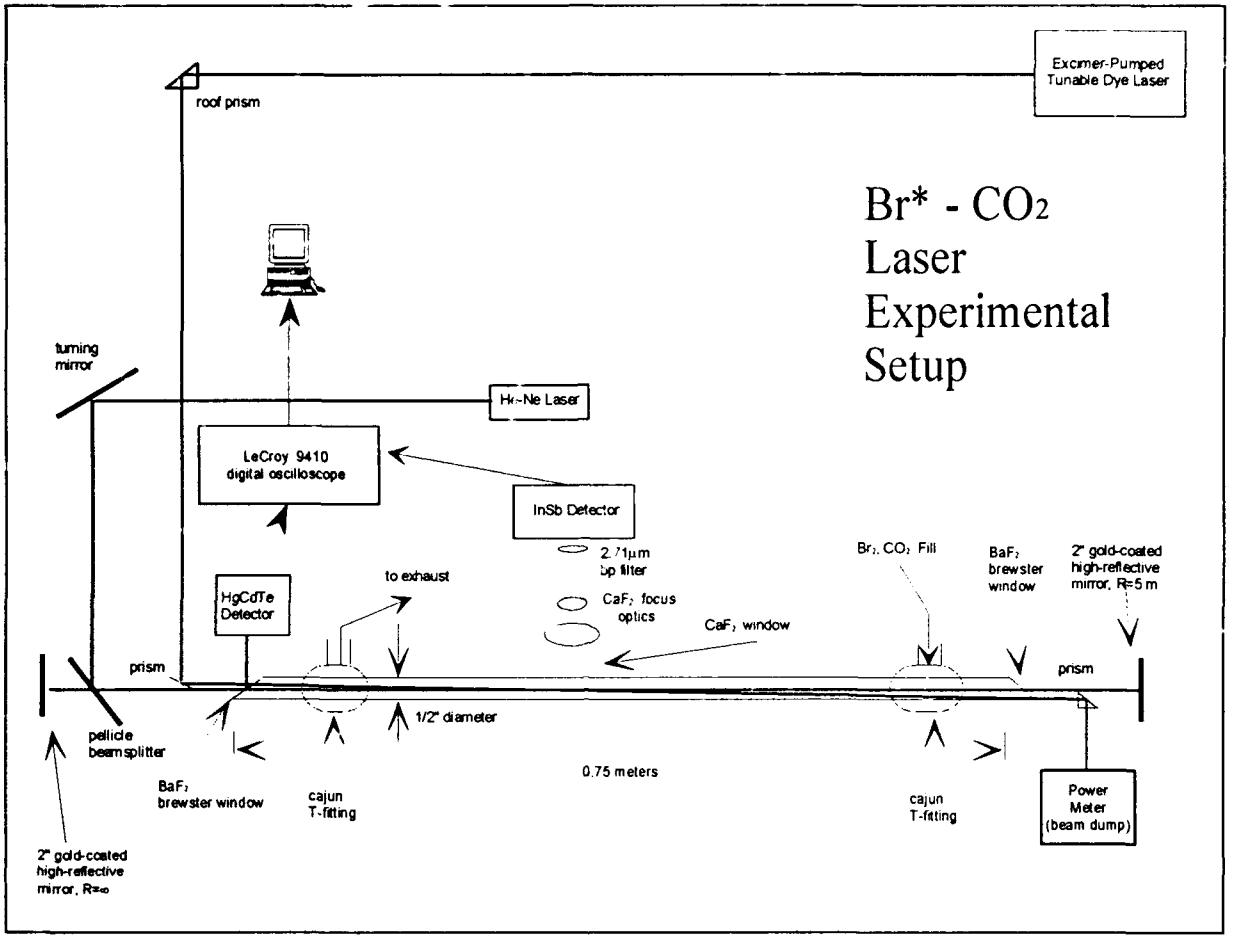

Figure 1.1 Proposed Experimental Apparatus

An excimer laser operating at 308 nm will be used to pump a dye laser, which, in turn, is used as the photolysis pump source. A dye will be selected to maximize Br_2 absorption of the pump beam. Molecular bromine will be introduced into the reaction cell via an appropriate gas handling apparatus. The gas handling apparatus is currently in situ, serving the needs of another related experiment. Similar to the Pastel *et al.* work, the pump beam is introduced into the resonator by a series of right angle prisms. The pump beam axis will be slightly offset from the lasing axis to prevent damage to cavity mirrors. A 4 mW helium-neon laser is available to aid in this alignment. Initially, bromine alone will be introduced into the cell, and detection of Br* fluorescence accomplished with a side-viewing InSb detector equipped with a 2.71 μm interference filter to mask molecular

fluorescence present, if any. Confirmation of previous work on parent molecule quenching of Br* will be reproduced. CO_2 will then be introduced into the cavity cell at a starting pressure of 10% of $[Br_2]$. A fast HgCdTe detector will be used to view the 4.3 μm line off the first CaF_2 brewster window. Once lasing is achieved, system operation will be investigated for a variety of gas mixtures, gain medium lengths, etc.

Summary

This completes the introductory portion of this thesis. Chapter II will describe the theory involved with this experiment; Chapter III will describe the experimental setup in more depth. Chapters IV and V will concentrate on the experimental procedures and results that were obtained. Chapter VI will present any conclusions reached as a result of this effort, and recommendations for future work in this area.

II. Theory

Introduction

We now summarize the basic theory inherent in the E⇨V energy transfer process and some fundamental laser development theory key to this effort. The first section describes, briefly, the structure of the Br_2 molecule and its propensity to dissociate in the presence of light energy. The second section discusses the gas kinetic processes at work, and the third and final theory section examines the predicted gain of the Br* - CO_2 laser and compares the theoretical value to the required threshold inversion.

Molecular Bromine Description

Bromine occurs naturally as a diatomic molecule with two stable isotopes, ^{79}Br and ^{81}Br, which exist in nearly equal abundance. When two bromine atoms are brought together to form a bromine molecule, there are certain attractive and repulsive forces present which serve to maintain an equilibrium positioning of the two atoms. Figure 2.1 shows a potential energy diagram for Br_2 and illustrates the various molecular energy states. The ground state of the bromine molecule is represented by convention as the X state and is spectroscopically identified as $^1\Sigma$ (read as singlet sigma). Excited states of increasing energy are subsequently designated A, B, C,... and given the $^3\Pi$ (triplet pi) spectroscopic notation. The labeling of these molecular quantum states, in general, proceeds from the basic notation

$$^{2\Sigma+1}\Lambda_{\Omega} \qquad (2.1)$$

where the $2\Sigma+1$ superscript is the state multiplicity and the Ω subscript yields the multiplet component. Λ is the quantum number associated with the orbital angular

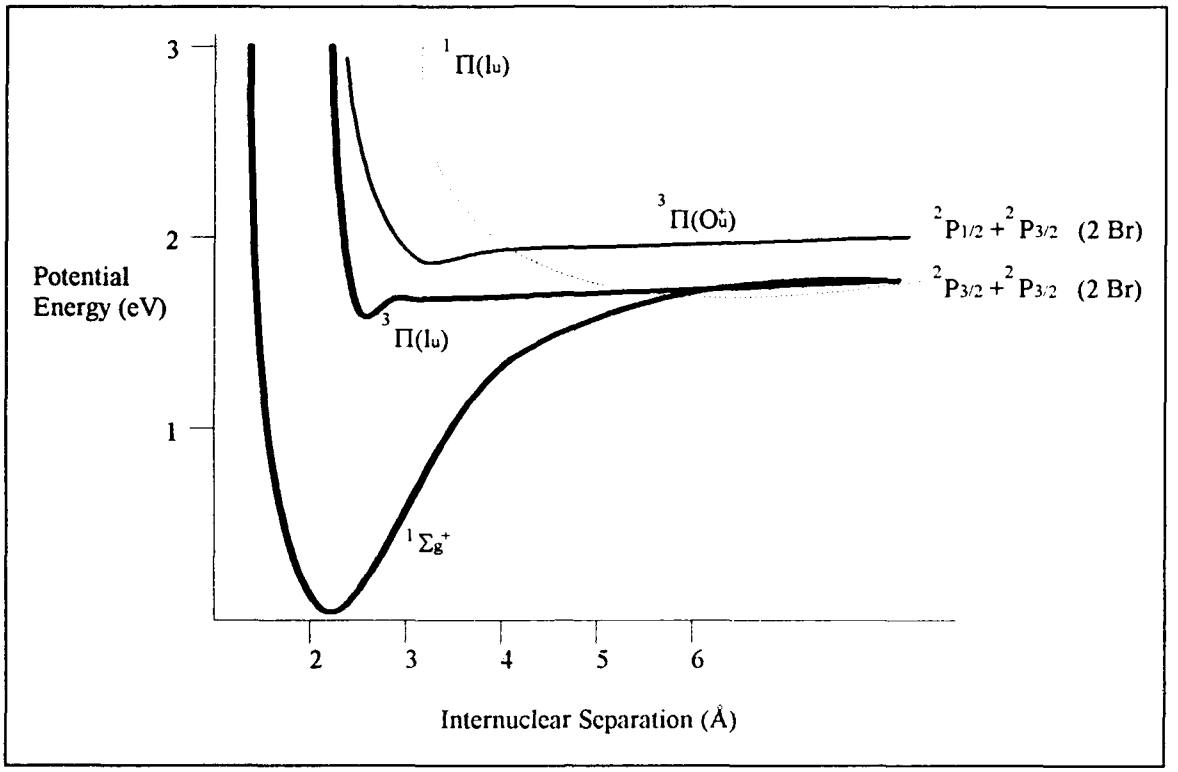

Figure 2.1 Br_2 Potential Energy Diagram (10:28)

momentum ($\Lambda = |M_L|$) and can take on values $\Lambda = 0, 1, 2,...L$. These values correspond to $\Lambda = \Sigma, \Pi, \Delta, \Phi,...$ M_L is the component of the electron angular momentum and can take on values $M_L = L, L-1, L-2,..., -L$. For Br_2, $L = 1$ and $\Lambda = \Sigma$ and Π (12:26).

In Figure 2.1, the first few excited states of Br_2 are represented, with the bound states shown as bold solid curves, and the unbound or repulsive states identified by dotted curves. If sufficient energy is absorbed by the bromine molecule, dissociation occurs and results in either a Br* atom and a ground state atom (upper solid curve) or two ground state atoms.

The wavelength regime over which photodissociation of bromine occurs has been measured. Photolysis occurs readily for light absorbed with $450 \leq \lambda \leq 530$ nm and results in approximately equal amounts of Br* and ground state bromine atoms (11:1052).

Photon energies greater than 450 nm generally result in the accessing of unbound states and follows the creation of two ground state atoms (12:16). Photolysis at 488 nm results in a peak quantum yield of 84% (12:18). The full details of the photolysis process have been described elsewhere (12:14-19).

Once photodissociation takes place, two bromine atoms, $Br(^2P_{1/2})$ and $Br(^2P_{3/2})$, are the result. Figure 2.2 displays the energy separation (fine and hyperfine structure) of the two states.

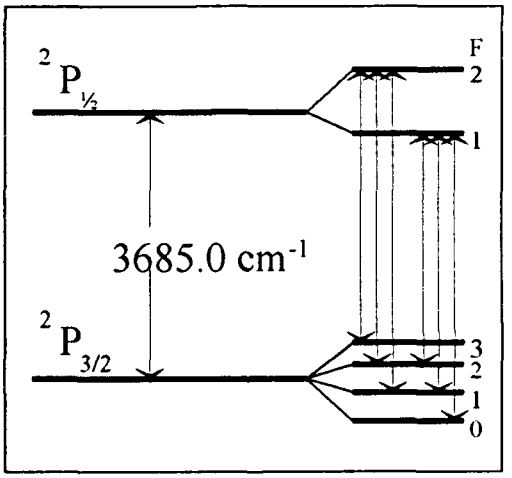

Figure 2.2 Bromine Atomic Energy Level Diagram

The diagram shows the energy difference between the excited and ground states (fine structure) and the allowed transitions between the hyperfine states, $\Delta F = 0, \pm 1$. The energy difference of 3685 cm^{-1} corresponds to a transition wavelength of 2.714 μm. Hyperfine transitions as a result of nuciear spin will not be visible in this experiment as the 2.71 μm filter FWHM bandwidth of approximately 0.02 μm (27 cm^{-1}) is not sufficient to isolate these transitions. The 300K Doppler line width of these hyperfine transitions is approximately 0.0051 cm^{-1} or 150 MHz.

Gas Kinetic Theory

Excited state bromine atoms ($Br(^2P_{1/2})$) can relax to the ground state through either radiative or non-radiative transitions. Radiative transitions result in spontaneous photon emission at 2.71 μm as previously described. Non-radiative transitions result from a variety of collisional deactivation processes, and do not result in emitted photons. For radiative transitions, a straightforward relationship applies:

$$Br^* \xrightarrow{k_R} Br + h\nu \tag{2.2}$$

where k_R is the radiative rate, and hν is the energy contained in the 2.71 μm emitted photon.

Non-radiative transitions generally result from collisions of an excited state atom or molecule with other particles, or with the container walls. For this analysis, it is assumed wall deactivation of Br* to be negligible compared to other processes. In general, the collisional deactivation sequence is described by

$$Br^* + M \xrightarrow{k_Q} Br + M^\circ \tag{2.3}$$

where M represents the specific collisional partner, k_Q is the quenching rate with respect to Br*, and M° is the resultant excited collisional partner (1:4456). This equation does not completely describe the collision process, however. Energy may be transferred to the collisional partner in the form of translational, rotational, or vibrational excitation (12:32).

Before examining the E⇨V energy transfer process, we seek to understand the lifetime of the Br* atom and contributing factors. The time-dependent rate equation for Br* can be described in terms of collisional deactivation and radiative processes:

$$\frac{d[Br^*]}{dt} = k_p[Br_2] - k_R[Br^*] - k_{Br_2}[Br_2][Br^*] - k_Q[M][Br^*] \qquad (2.4)$$

where

$[Br_2]$ = Br_2 concentration (molecules cm^{-3})

$[Br^*]$ = Br* concentration (atoms cm^{-3})

[M] = concentration of quenching species (molecules cm^{-3})

k_p = pump rate coefficient (cm^2 $watt^{-1}$ sec^{-1})

k_{Br_2}, k_Q = quenching rate coefficients (molecules^{-1} cm^3 sec^{-1})

k_R = radiative rate (sec^{-1})

For the situation where no other gases are present, the last term in (2.4) is dropped and we have

$$\frac{d[Br^*]}{dt} = k_p[Br_2] - k_R[Br^*] - k_{Br_2}[Br_2][Br^*] \qquad (2.5)$$

This a standard linear first order differential equation which can be solved with established techniques. To solve this equation and subsequent differential equations in this paper, Mathematica for Windows Version 2.0 was used. For CW operations, a steady-state condition is achieved, so (2.5) is set equal to zero, and solved for [Br*]:

$$[Br^*] = \frac{k_p[Br_2]}{k_R + k_{Br_2}[Br_2]} \qquad (2.6)$$

For pulsed photolysis, the creation of Br* on the time scale of interest is nearly instantaneous, and we must discover an alternate approach to recovering the concentration of Br*, and hence its lifetime. Returning to (2.5), we factor out [Br*] to yield

$$\frac{d[Br^*]}{dt} = -\left(k_R + k_{Br_2}[Br_2]\right)[Br^*] = -\Gamma[Br^*] \tag{2.7}$$

where Γ is the equivalent rate coefficient for all relevant processes. Since we are interested in determining the Br* lifetime, and hence the absolute rate coefficient for quenching, we are not concerned with the creation of Br*, only its decay. Thus, the pumping term from (2.5) has been dropped. (2.7) is integrated to yield

$$[Br^*] = [Br^*]_{t=0} e^{-\Gamma t} \tag{2.8}$$

As expected, a single exponential time decay is the result. Γ can be plotted vs. Br_2 pressure in the form of a Stern-Volmer plot to obtain the rate coefficient for Br* deactivation.

We now consider kinetics after adding CO_2 to the equation. The Br* concentration is still described by the solution to (2.4), but the concentrations of the various states of CO_2 require considering the E⇨V energy transfer process from Br*. The quenching of electronically-excited Br* atoms has been extensively studied. For those species that are efficient quenchers of Br*, the E⇨V energy transfer mechanism has been shown to be the major pathway (1:4454). When a collision takes place between a Br* atom and a collision partner, in this case CO_2, electronic energy from the Br* atom is transferred to the CO_2 molecule and excites vibrational modes at near-resonant energy levels with

respect to Br* (3685 cm^{-1}). Depending on their energy levels, several excited vibrational states of CO_2 may result from Br* E⇨V transfer. Due to their near-resonant energy, the [101] and [021] states are the most likely candidates (11:1053). The chemical reaction which results in generation of [101] is described by

$$Br^* + CO_2[000] \rightarrow Br + CO_2[101] - 30\,cm^{-1} \qquad (2.9)$$

Figure 2.3 graphically illustrates the E⇨V transfer path and shows the first few vibrational levels of CO_2:

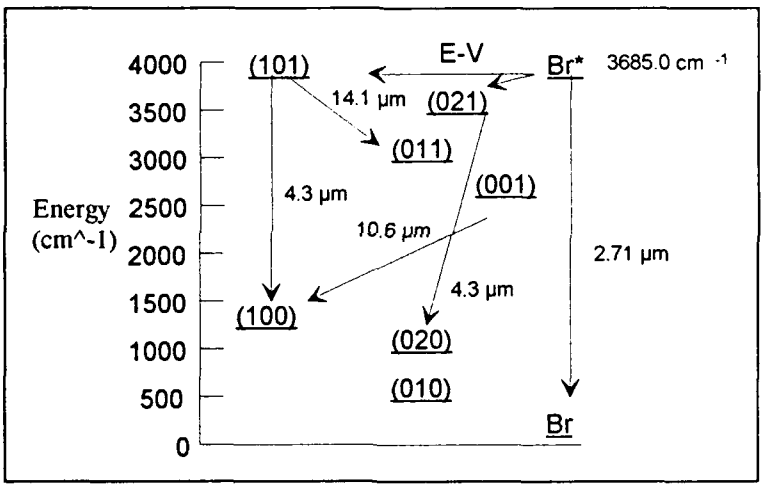

Figure 2.3 CO_2 Energy Level Diagram

Radiative transitions from the [101] to the [100] level at 4.3 µm may result after the E⇨V process takes place.

Br - CO_2 Laser Calculations*

It is the creation of excited CO_2 that leads to possible stimulated emission activity. It must be determined whether or not threshold conditions for lasing can be achieved. The

full extent of the experimental apparatus will be described later, so for the purposes of this analysis only essential hardware will be mentioned.

Examinining first the threshold lasing conditions that must be met by calculating the threshold gain for this cavity, the minimum gain which must be achieved is a function of cavity dimensions and optical properties (assuming no or negligent scatterring losses):

$$T_{BW}^{4} R_1 R_2 e^{2 l_g \gamma_{th}(\nu)} \geq 1 \tag{2.10}$$

where T_{BW} is the transmissivity of the brewster windows on either end of gas reaction cell (gain medium), R_1 and R_2 are the cavity mirror reflectivities, l_g is the length of the gain medium, and $\gamma_{th}(\nu)$ is the threshold gain coefficient. Solving for $\gamma_{th}(\nu)$,

$$\gamma_{th}(\nu) = \frac{1}{2 l_g} \ln\left(\frac{1}{T_{BW}^{4} R_1 R_2}\right) \tag{2.11}$$

For this proposed experimental effort (the experimental parameters are discussed in detail in a later section)

$$T_{BW} = 0.985$$

$$R_1 = R_2 = 0.99$$

$$l_g = 118 \text{ cm}$$

the minimum gain which will support stimulated emission is $\gamma_{th}(\nu) \geq 3.4134 \times 10^{-4} \text{ cm}^{-1}$.

The gain of any laser system is a function of the populations of the upper and lower laser levels and stimulated emission cross section for the transition:

$$\gamma_o(\nu) = \Delta N \sigma_{SE}(\nu) \tag{2.12}$$

$$\Delta N = N_2 - \frac{g_2}{g_1} N_1 \tag{2.13}$$

where $\gamma_o(\nu)$ is the gain in cm^{-1}, ΔN is the population inversion in cm^{-3}, $\sigma_{SE}(\nu)$ is the stimulated emission cross section in cm^2, and g_1 and g_2 are the degeneracies of the lower and upper laser levels, respectively. To calculate the lower and upper level populations, we need to examine the kinetics associated with the [101] (upper level) and [100] (lower level) states of CO_2. The production of [101] is related to the concentration of Br* and quenching reactions:

$$\frac{d[101]}{dt} = k_{EV}[Br^*][000] - k_{[000]-[101]}[000][101] - k_{Br_2-[101]}[Br_2][101] \tag{2.14}$$

where

k_{EV} = E⇨V rate coefficient ($cm^3\ sec^{-1}$)

$k_{[000]-[101]}$ = [000] on [101] quenching rate coefficient ($cm^3\ sec^{-1}$)

$k_{Br_2-[101]}$ = $[Br_2]$ on [101] quenching rate coefficient ($cm^3\ sec^{-1}$)

The other factors in the equation are as previously defined, and [Br*] is calculated using (2.8). Integrating both sides of (2.14),

$$[101] = \frac{[Br^*]_{t=0} \exp\left(-[Br_2]k_{Br_2-[101]}t - [000]k_{[000]-[101]}t - \Gamma t\right)\left[\exp\left([Br_2]k_{Br_2-[101]}t + [000]k_{[000]-[101]}t\right) - \exp(\Gamma t)\right]}{\frac{[000]k_{[000]-[101]}}{\Gamma} + \frac{[Br_2]k_{Br_2-[101]}}{\Gamma} - 1}$$

$$\times \frac{[000]k_{EV}}{[000]k_{[000]-[101]} + [Br_2]k_{Br_2-[101]} - \Gamma} \tag{2.19}$$

The literature values for the various rate coefficients are

$k_{[000]-[101]} = 1.3\times10^{-10}\ cm^3\ molecule^{-1}\ sec^{-1}$

$k_{Br_2-[101]} = 8\times10^{-15}\ cm^3\ molecule^{-1}\ sec^{-1}$ †

$k_{EV} = 6.0\times10^{-11}$ cm^3 molecule^{-1} sec^{-1}

† The rate coefficient for quenching of [101] by Br_2 has not been reported, but the Br_2 quenching rate on a nearby vibrational level ([001]) is slow (8×10^{-15} cm^3 sec^{-1}). We include this rate in the analysis, although the effect is minimal.

The Br* lifetime rate coefficient, Γ, is related to quenching of Br* by [000] and Br_2

$$\Gamma = \left(k_{Br_2-Br^*}[Br_2] + k_{CO_2-Br^*}[000]\right) \tag{2.20}$$

where $k_{Br_2-Br^*} = 4.8\times10^{-13}$ cm^3 sec^{-1} and $k_{CO_2-Br^*} = 1.5\times10^{-11}$ cm^3 sec^{-1}. Gas concentrations chosen for this analysis:

$[Br_2] = 0.8$ torr

[000] = 0.25 torr

This leaves only one parameter to calculate--the initial concentration of Br*. The number of Br* atoms produced will be directly proportional to the number of pump photons absorbed by the Br_2 in the gain medium. Absorption of pump photons along the gain medium path length obeys the Beer-Lambert law:

$$I_{absorbed} = I_p - I_t \tag{2.21}$$

$$I_t = I_p e^{-\sigma_{Br} l_g [Br_2]} \tag{2.22}$$

where

$I_{absorbed}$ = absorbed pump laser intensity (watts cm^{-2})

I_p = pump laser intensity (watts cm^{-2})

I_t = transmitted pump laser intensity (watts cm^{-2})

σ_{Br} = absorption cross section of Br_2 (cm^2)

For a 2 mm diameter pump beam and an average pump power at the cavity entrance of 62 mW, we obtain an average pump intensity of

$$I_p = \frac{62\text{mW}}{\pi(.1\text{cm})^2} = 1.974\frac{\text{W}}{\text{cm}^2} \tag{2.23}$$

and the transmitted intensity

$$I_t = 1.974e^{-(1.55\times10^{-19})(118)(3.22\times10^{16})(0.8)} = 1.2323\frac{\text{W}}{\text{cm}^2} \tag{2.24}$$

The value for the absorption cross section of Br_2 comes from previous work (Johnson). Thus, the absorbed intensity is 1.974 - 1.2323 = 0.7417 W/cm^2. To get the total number of photons absorbed per unit volume, and hence the concentration of [Br*] at time t = 0,

$$[Br^*]_{t=0} = \frac{E_{absorbed}}{Al_g h\nu}\Phi(\lambda) \tag{2.25}$$

$$E_{absorbed} = \frac{I_{absorbed}\cdot A}{\nu_r} \tag{2.26}$$

where A is the cross-sectional area of the pump beam, $\Phi(\lambda)$ is the photon yield of Br*, ν_r is the pulse repetition rate and $h\nu$ is pump photon energy. For a photon yield of 0.8 (2:3408) and a pulse repetition rate of 25 Hz,

$$[Br^*]_{t=0} = \frac{(0.7417)(0.8)}{(118)(25)(6.6262\times10^{-34})(6.98\times10^{13})} = 4.3489\times10^{15}\,\text{cm}^{-3} \tag{2.27}$$

Reducing (2.19) to an exponential function of time by substituting calculated values yields

$$[101] = 6.4818\times10^{14}\left(e^{-1.3311\cdot10^{5}t} - e^{-1.0467\cdot10^{6}t}\right) \tag{2.28}$$

Figure 2.4 shows the evolution of [101] with time:

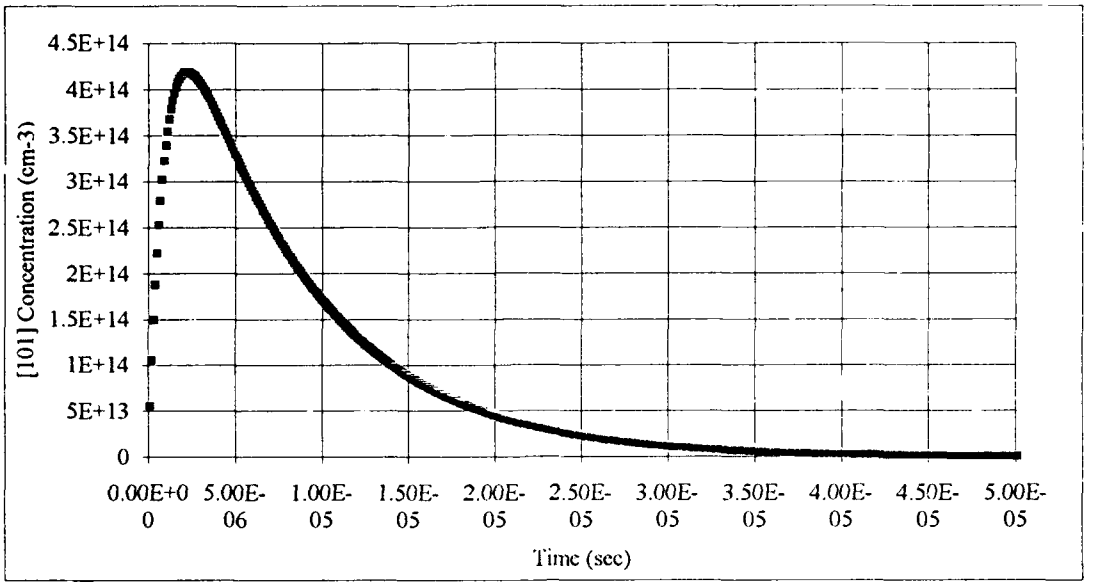

Figure 2.4 Time Evolution of the Upper Laser Level Population

The lower laser level ([100]) population at threshold is the product of the ground state population ([000]) times the Boltzmann fraction:

$$[100]_0 = e^{\frac{-\Delta E}{kT}}[000] \tag{2.30}$$

where ΔE is energy difference between the [100] level and the ground state. For the [100] vibrational level, $\Delta E = 1351\ cm^{-1}$. This yields a lower laser level population of

$$[100] = e^{\frac{-1351}{208}}(0.25)(3.22 \times 10^{16}) = 1.22 \times 10^{13}\,cm^{-3}$$

The purpose of examining the population of the two laser levels is to determine whether a suitable population inversion is present. Looking at Figure 2.4, during the time frame of

interest (around 200-300 nsec), $[101] \approx 4 \times 10^{14}$ cm^{-3}. This leads to a population inversion of

$$\Delta N = 4 \times 10^{14} - 1.22 \times 10^{13} = 3.88 \times 10^{14}\,\mathrm{cm}^{-3} \tag{2.32}$$

Half of (2.12) is now evaluated. Determining the stimulated emission cross section for the [101] - [100] transition is the next step. For any transition, the stimulated emission cross section is directly related to the transition line shape:

$$\sigma_{SE} = A_{21} \frac{\lambda^2}{8\pi n^2} g(\nu_o) \tag{2.33}$$

where $g(\nu_o)$ is the transition line shape, λ is the transition wavelength, and n is the gain medium index of refraction. The transition line shape arises from a Doppler-broadened medium (low pressure operation):

$$g(\nu_o) = \sqrt{\frac{4\ln 2}{\pi}} \frac{1}{\Delta\nu_D} \tag{2.34}$$

$$\Delta\nu_D = 7.13 \times 10^{-7} \sqrt{\frac{T}{m}} \nu_o \tag{2.35}$$

$\Delta\nu_D$ is the Doppler transition width, T is the gas temperature, m is the mass of the lasing medium in atomic mass units, and ν_o is the center frequency of the transition. Using appropriate values,

$$g(\nu_o) = \sqrt{\frac{4\ln 2}{\pi}} \left(7.13 \times 10^{-7} \sqrt{\frac{300}{44}} 6.98 \times 10^{13} \right)^{-1} = 7.2264 \times 10^{-9}\,\mathrm{Hz}^{-1} \tag{2.36}$$

and

$$\sigma_{SE} = 0.18\frac{4.3\times10^{-6}}{8\pi(1)^2}7.2264\times10^{-9} = 9.5696\times10^{-18}\,\mathrm{cm}^2 \qquad (2.37)$$

where the value for A_{21} comes from a nearby transition ([001] - [000]), as the A coefficient for the transition of interest was not available. Returning now to (2.12),

$$\gamma_o(\nu) = \left(3.88\times10^{14}\right)\left(9.5696\times10^{-18}\right) = 3.711\times10^{-3}\,\mathrm{cm}^{-1} \qquad (2.38)$$

Comparing this value to the result for the required threshold gain from (2.11), $\gamma_{th} = 3.413\times10^{-4}$ cm^{-1}, observe that we are above threshold by an order of magnitude. The final investigation involves examining the distribution of rotational lines within the [101] ibrational level. Lasing may take place on a variety of these ro-vibrational transitions. The thermal distribution of rotational levels is according to Boltzmann given by

$$n_{vJ} \cong N_v\left(\frac{2hcB}{kT}\right)(2J+1)e^{\left[-F(J)\frac{hc}{kT}\right]} \qquad (2.39)$$

where N_v is the total number of molecules per unit volume having a particular vibrational state, J is the rotational number, and F(J) the rotational energy is given by

$$F(J) = B_vJ(J+1) - D_vJ^2(J+1)^2 \qquad (2.40)$$

where B_v and D_v are rotational constants which vary slightly for different rotational levels (15:16-17). In general, D_v is much smaller than the B coefficients and is neglected here. In addition, for CO_2, $B \cong B_v = 0.3896$ cm^{-1} (4:395). (2.39) is plotted in Figure 2.5 and shows the distribution of rotational levels.

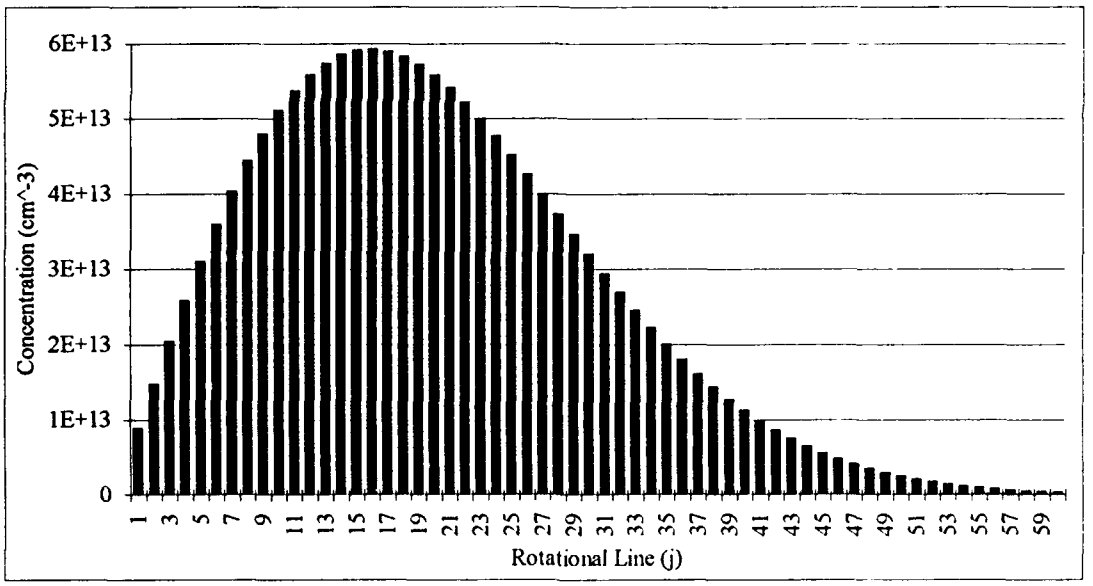

Figure 2.5 Rotational Line Distribution

It may be useful as well to determine which rotational line is most likely to lase:

$$J_{max} \cong \sqrt{\frac{kT}{2Bhc}} - \frac{1}{2} \cong 16 \qquad (2.41)$$

which is also evident from the figure. Additionally, the rotational partition function determines the distribution of energy into the various rotational levels. Thus there are many rotational lines which may accept the transferred energy from the Br*, and this further decreases the efficiency of the process. The true population of the upper laser level (and hence the cavity gain) must be adjusted accordingly. Looking at Figure 2.6, the population of the J =16 rotational line is ~ 6×10^{13} cm^{-3}. If we use this value for the population of the upper laser level in (2.32),

$$\Delta N = 6\times10^{13} - 1.22\times10^{13} = 4.78\times10^{13}\,cm^{-3}$$

This yields

$$\gamma_o(\nu) = (4.78 \times 10^{13})(9.5696 \times 10^{-18}) = 4.574 \times 10^{-3}\,\mathrm{cm}^{-1}$$

Now we're operating at the ragged edge of threshold, above γ_{th} by only a factor of 1.34. The most suspect parameter, however, is the A coefficient for the [101] - [100] transition, used in the calculation of σ_{SE}. We've chosen a very conservative value (0.18 sec^{-1})--a more realistic rate will only help our gain. We conclude that lasing--on the basis of the above calculations--should be possible.

III. Experimental Apparatus

Introduction

This chapter describes the experimental hardware used in this research effort. Major subsystems discussed include the pump laser subsystem, the resonator, the detectors, and the gas handling apparatus.

The experimental apparatus used in this research is illustrated in Figure 3.1.

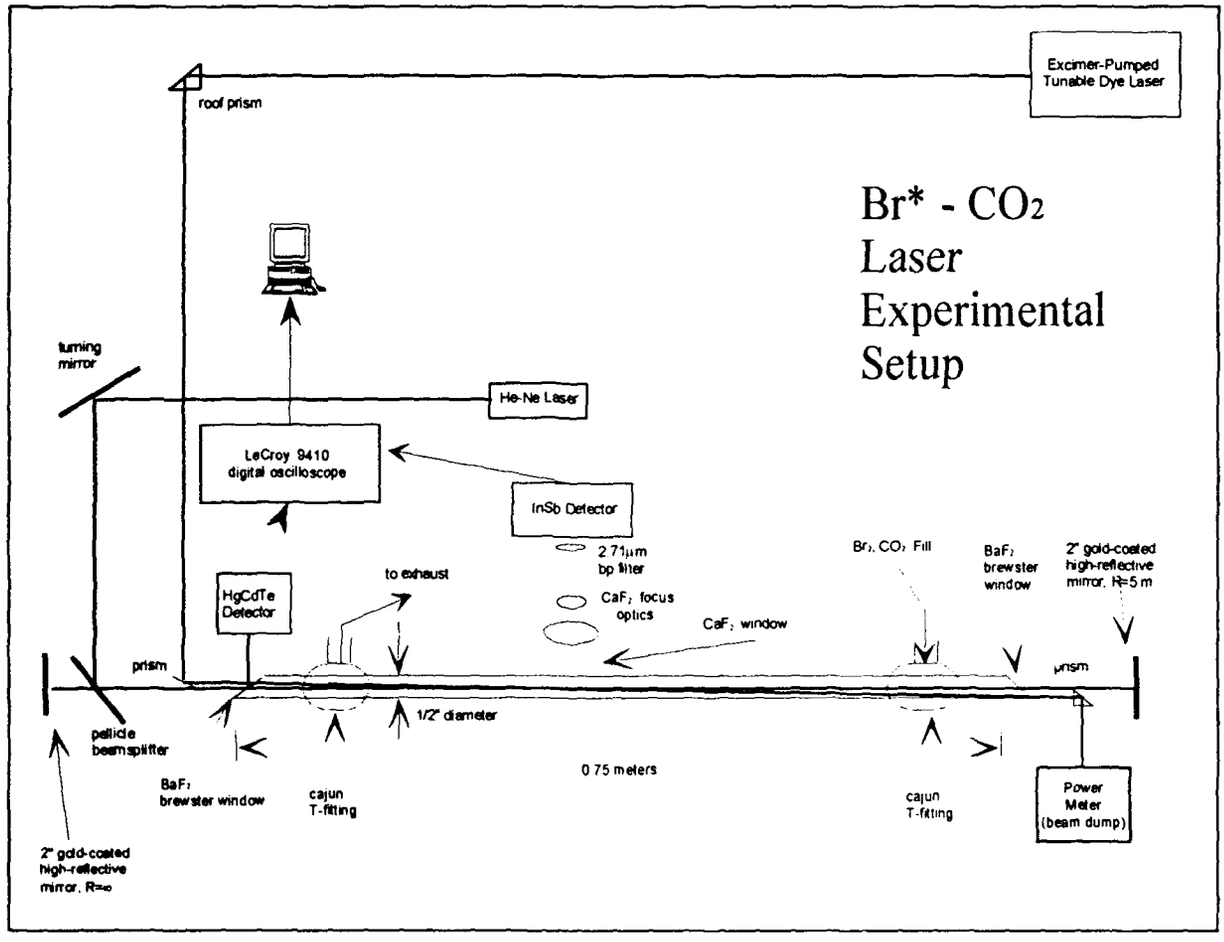

Figure 3.1 Experimental Apparatus

Main Cavity Design

A simplistic cavity design promotes engineering flexibility. The central laser tube consists of ½-inch outer diameter pyrex glass, approximately 118 cm long, sealed off at both ends with infrared-passing Oriel CaF_2 windows oriented at Brewster's angles to the lasing axis. This orientation of the windows allows maximum transmission of both the pump and CO_2 beams. Approximately 5 cm from the first brewster window, the laser tube is expanded to 2 inches outer diameter to enhance side-viewing of Br* fluorescence. An Oriel pellicle beamsplitter to the left of the first brewster window directs a He-Ne laser beam for cavity alignment purposes. The resonator subsystem is completed by two CVI Laser Corp. gold-coated high-reflectivity ($r > 0.99$) mirrors. The left mirror is flat ($R = \infty$); the right mirror slightly curved ($R = 5$ m) to aid cavity alignment.

Pump Laser Subsystem

The pump laser consists of a Lambda Physik FL 3002 pulsed dye laser, pumped by a Lambda Physik EMG 101-104 MSC excimer laser, operating at the XeCl wavelength of 308 nm. The dye for the FL 3002 (Coumarin 480 ⇳ $\lambda_{peak} = 480$ nm) was chosen so as to maximize photon absorption by Br_2. The pump beam is directed into the laser cavity by a series of four right-angle prisms. A fifth prism at the right end shunts the beam out of the cavity to avoid damage to the mirrors. The nominal average pump pulse power at a pulse repetition rate of 25 Hz achieved for this experiment *at the first brewster window* is ~ 60 mW. FWHM pulse width is ~ 40 nsec.

Detector Subsystem

Two detectors are positioned to provide evidence of Br* production and CO_2 lasing. A EG&G-Judson model J10D-M204-R02M-60 InSb detector is used to view Br* fluorescence from the side. A CaF_2 window passes the 2.71 μm Br* signal, and two CaF_2 lenses collect and focus that signal onto the InSb detector. The detector itself has an

active area of 4 mm^2, D* = 1.84×10^{11} cm - $Hz^{1/2}/W$, and is ~ 40% responsive at 2.71 μm. A sapphire window in front of the detector passes IR, and wide and narrowband interference filters are used select individual wavelengths. Output coupling of the CO_2 beam is detected off the first brewster window with a Kolmar Technologies model KV103-0.1-A-2-2SMA(.2) HgCdTe detector. This detector has a much faster response time ($\sim 10^{-8}$ sec), to permit time resolving of the CO_2 laser pulse. Detector D* = 3.88×10^{10} cm $Hz^{1/2}/W$, is ~ 70% quantum efficient at 4.3 μm, and has two elements with active areas of 0.2 and 0.1 mm^2, respectively. Bandwidth of the detector is > 100 MHz. Both detectors are cooled to 77K with LN_2. Detector outputs are sent to a LeCroy 9410 digital oscilloscope for analysis. An RS-232C connection to a Zenith 248 PC provides further analysis and archival opportunities.

Gas Handling

The gas containment apparatus permits safe routine handling of the toxic bromine. Purification and disposal schemes have been described elsewhere (12:49-50). CO_2 is also fed into the system through this apparatus. Pressure in the reaction cell was continuously monitored via a Baratron MKS detection system. At 10-torr max pressure head inserted just to the right of the main reaction cell provided the continuous pressure reading. An ultimate vacuum of 0.5 mtorr in the reaction cell was routinely achieved. On-going leak monitoring indicated a maximum leak rate of ~ 0.2 mtorr per minute--within acceptable limits.

IV. Experimental Procedures

Introduction

This chapter discusses the various experimental procedures followed in obtaining the data presented in following chapters. Note that particular attention is paid to the procedure for positioning the two detectors used in the experiment.

Detector Alignment

Before any useful data can be taken, precise alignment of both the InSb and HgCdTe detectors must be accomplished. To position the InSb detector, a CW Br* signal is required. For this task only, a CW argon-ion laser operating at 488 nm is utilized. Figure 4.1 shows the CW setup:

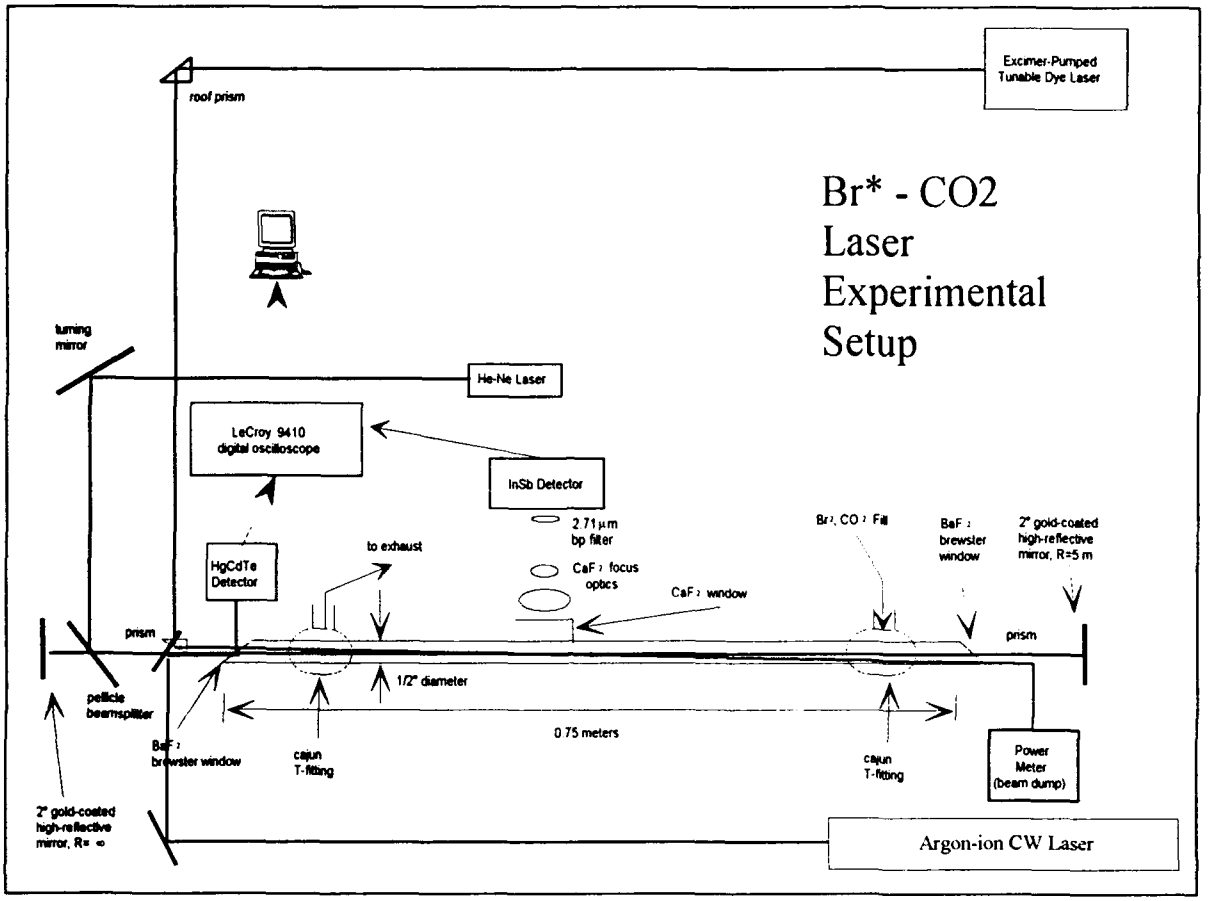

Figure 4.1 Detector Alignment Setup

The argon-ion laser outputs ~ 800 mW of 488 nm light, and is chopped at 200 Hz to provide synchronous detection just prior to insertion into the gain medium. A freon-based spray is sent down the length of the reaction cell via the gas disposal outlet. This allows the beam to be visible, permitting focusing of the beam onto the InSb detector element by moving either or both CaF_2 lenses and the detector. Once the desired positioning of the beam image onto the detector element is achieved, the cell is then sealed and prepared for bromine operations. Once a suitable vacuum is achieved in the reaction cell ($\leq$ 10 mtorr), Br_2 is flowed into the cell. The Br* fluorescence is detected; the output voltage from the detector displayed on a Stanford Research 510 lock-in amplifier. The SR510 is connected via an RS-232C port to a Zenith 248 PC for data reduction and storage. The detector is

then positioned using an X-Y micrometer stage for maximum signal. A typical signal strenght achieved is ~ 20 μV. Complete CW operations have been described elsewhere (12:49-55).

Br Fluorescence Data Procedure*

For pulsed operations, the normal pump laser path is restored, and both excimer and dye lasers are energized. Average power out of both lasers is monitored throughout the experiment. Prior to filling the cell with bromine, a background signal is collected. A 2.71 μm broadband (FWHM ~ 0.1 μm) interference filter is placed in front of the detector to keep out visible and near IR radiation. The LeCroy 9410 averages over 5000 shots to improve the signal-to-noise ratio (SNR). A fresh supply of bromine is then flowed into the cell, starting with an initial fill of 50 mtorr. After collecting the first series of data points, the averaged signal is stored, then the background signal is subtracted from this averaged signal to isolate the Br* signal. The averaged, background-subtracted Br* signal is then sent to the PC for later processing and analysis. This procedure is repeated for each incremental addition of bromine.

$CO_2^\dagger$ Fluorescence Data Procedure

The procedure for collecting $CO_2^\dagger$ data ([101] state) is similar to that for collecting the Br* data. A particular amount of bromine is loaded into the cell (nominally ~ 0.8 torr), and CO_2 is then added in 50 mtorr increments, beginning with 50 mtorr. The signal is collected on the InSb detector and then passed to the LeCroy 9410 as previously. To view Br* fluorescence a narrowband (FWHM ~ 0.02 μm) interference filter is placed in front of the detector to mask the molecular fluorescence in the vicinity of 2.7 μm..

Br - CO_2 Laser Demonstration Procedure*

§ Cavity Alignment

For the laser demonstration, the helium-neon laser is required for cavity alignment purposes. Referring to Figure 4.1, the insertion path of the He-Ne beam is evident. The pellicle beamsplitter first brings the He-Ne beam into the resonator cavity. With adjustment of the pellicle, the He-Ne beam should pass as close as possible below the first prism in the cavity, and just above the second prism, and the spot should be visible on the right cavity mirror (an iris diaphragm is inserted in the beam path just to the right of the right brewster window to provide a sharper spot on the mirror. and to aid in the alignment procedure). Positioning the beam directly adjacent to the two turning prisms is necessary to maximize overlap of the CO_2 lasing axis and the pump beam. It is along this overlap region that Br* and, hence, [101] is created. Next, the return spot is located on the left cavity mirror. This return spot should overlap the initial reflection off the pellicle. Checks are made at each brewster window to insure overlap of all He-Ne beams. A final alignment verification is made by viewing the He-Ne spot as it passes directly through the pellicle onto the laboratory wall, and the reflection of the He-Ne beam after one round-trip through the cavity and reflected off the back surface of the pellicle onto the same wall. These two spots should precisely overlap. This insures the cavity is nearly aligned. Due to the beams nearly overlapping, the CO_2 beam should then travel the same path as the He-Ne. Lastly, the HgCdTe detector is positioned such that the He-Ne reflection off the first brewster window is centered onto the detector element. After the cavity alignment procedure has been performed, the pellicle is removed, as it degrades transmission of 4.3 μm radiation.

§ Laser Demonstration Procedure

After cavity alignment, the cell is filled with appropriate amounts of bromine and CO_2 per previously discussed procedures. The mixture which creates the strongest [101] signal is chosen for initial attempts. The pump beam is then allowed into the cell. At this point, the angle between the pump beam and the He-Ne beam is minimized to permit maximizing the Br* creation region. Br* + [101] creation is constantly monitored off the InSb detector. On a separate channel on the LeCroy 9410, the signal from the HgCdTe detector is monitored. If proper alignment has been achieved the CO_2 laser pulse should be evident, occurring some ~ 350 nsec after onset of photolysis (8:569). Most likely, the pulse will not be readily visible, and tweaking of the cavity optics will be necessary. Starting with the left cavity mirror, fine control of the X-Y positioning is adjusted in small increments, with the oscilloscope being constantly monitored. If lasing is not seen, the same procedure is applied to the right cavity mirror. Lasing should eventually be achieved. All data is then transferred to the PC for processing and archival as before.

V. Results

Introduction

This chapter presents the results of the experimental effort. First, lifetime data for Br_2 samples are examined, then the fluorescence data when CO_2 is added is analyzed and presented. Lastly, the Br*-CO_2 laser demonstration experimental data is reviewed.

Pulsed Fluorescence Data from Br_2 Samples

A representative signal utilizing the broadband interference filter (see Figure 6.1 for spectral characteristics) after photolysis of a Br_2 sample at 400 mtorr is shown in Figure 5.1. Unfortunately, the emission of Br* at 2.71 μm is very weak, and is likely to be masked by fluorescence from molecular impurities in the bromine sample, such as CO_2 at 4.3 μm. A narrowband filter is required to isolate the Br* emission. Experiments are in progress to accomplish this task. In the interim, we report the results using the broadband filter.

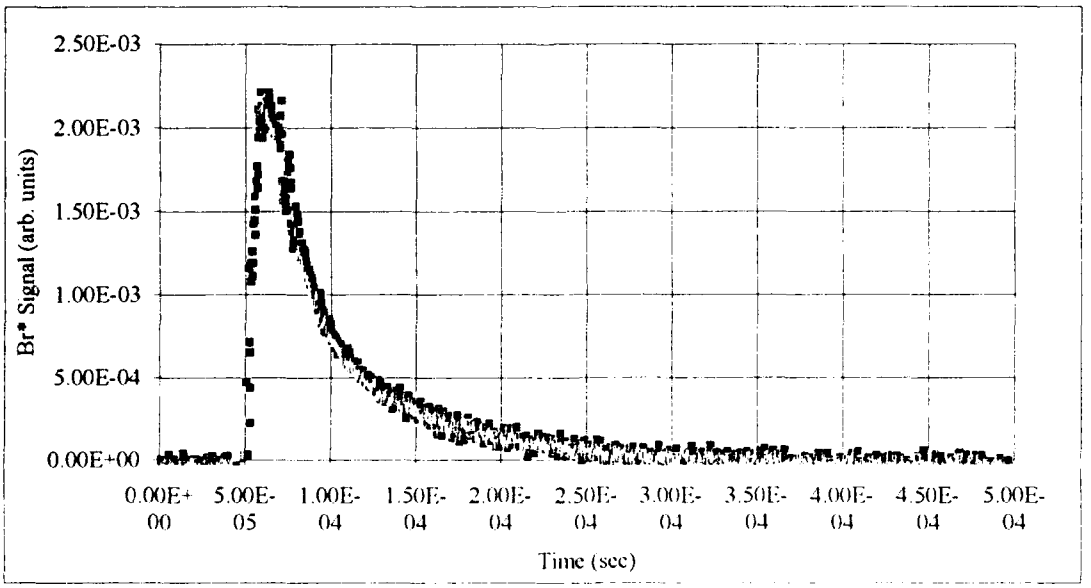

Figure 5.1 Br* Fluorescence Data

To characterize the exponential decay of the Br* concentration, we construct a table of values consisting of the slope of the lines created by taking the natural logarithm of the decay portion for each data set. Table 5.1 shows the slope values for each bromine pressure. The slope values were obtained by performing a linear fit to the log data using TableCurve.

Bromine Pressure	Fitted Slope from TableCurve (sec^{-1})
0.5 torr	3483
1.0 torr	8878
1.5 torr	8190
2.0 torr	14065
2.5 torr	16510
3.0 torr	18928
3.5 torr	20787
4.0 torr	24203
4.5 torr	26393
5.0 torr	27204

Table 5.1 Fitted Slope Values (Stern-Volmer Analysis) for Decay of IR Emission from Photolysis of Br_2

By plotting the above values and examining the slope of the fitted line to these values, we obtain an effective rate coefficient. Figure 5.2 shows the plotted data and straight line fit.

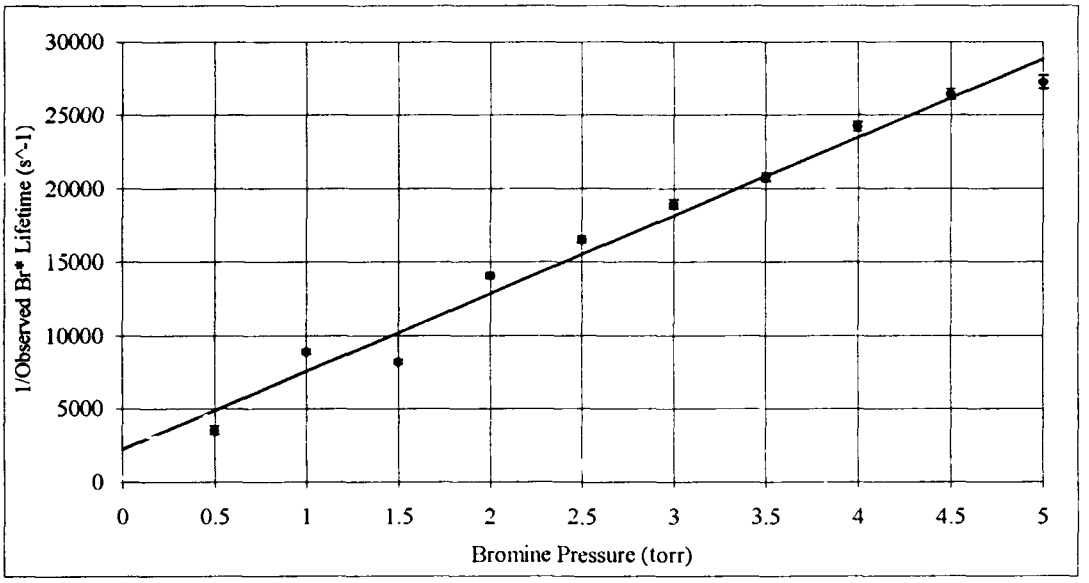

Figure 5.2 Stern - Volmer Fluorescence Lifetime Rate Analysis

The equation of the fitted line is

$$y = 2239.3333 + 5318.097x \tag{5.1}$$

The r^2 fitting coefficient for the data is 0.9767. Although not quite visible on the plot, the slight vertical extent of each data point represents the 95% confidence limits (error bars) for that measurement. The rate coefficient is derived by dividing the slope of the line by the number of bromine molecules per cm^3 per torr of gas:

$$k_1 = \frac{5318.097}{3.22 \times 10^{16}} = 1.6516 \times 10^{-13} \frac{cm^3}{sec \cdot molecule} \tag{5.2}$$

This rate is somehat similar to the published rate of 4.8×10^{-13} cm^3 sec^{-1} for quenching of Br* by Br_2 (6:317). Possible scenarios for variance from this rate are discussed in the next section.

A fit was also attempted using a double exponential functional form. If the observed emission is Br*, then the proposed rate equations predict the Br* to be created on a virtually instantaneous time scale; however it was apparent from the data collected that there was a definite, finite, pressure-dependent rise time of the signal. This implies that some other mechanism is affecting either the production or quenching of the observed emission. A standard double exponential is assumed:

$$y = a\left(e^{-bx} - e^{-cx}\right) \tag{5.3}$$

Table 5.2 shows the fit results obtained from TableCurve.

Br_2 Pressure	"b" coefficient	"c" coefficient	r^2 fit coefficient
0.5 torr	5203.42406	31478.0972	0.9180779956
1.0 torr	7366.96466	56969.6646	0.9741768533
1.5 torr	10384.5025	85090.7191	0.9698042757
2.0 torr	12337.4432	87696.8225	0.9652559551
2.5 torr	14830.3842	147742.393	0.9733257727
3.0 torr	19085.2268	108941.592	0.956794633
3.5 torr	20497.4022	193525.533	0.9761688113
4.0 torr	25257.5028	201751.238	0.9762902327
4.5 torr	27893.1137	220429.659	0.9731767912
5.0 torr	31493.7576	133928.031	0.9383705335

Table 5.2 Fluorescence Data Double Exponential Fit Parameters

We can apply again the Stern-Volmer analysis to each set of coefficients to obtain rate information. Figure 5.3 displays the linear fit of the "b" coefficients:

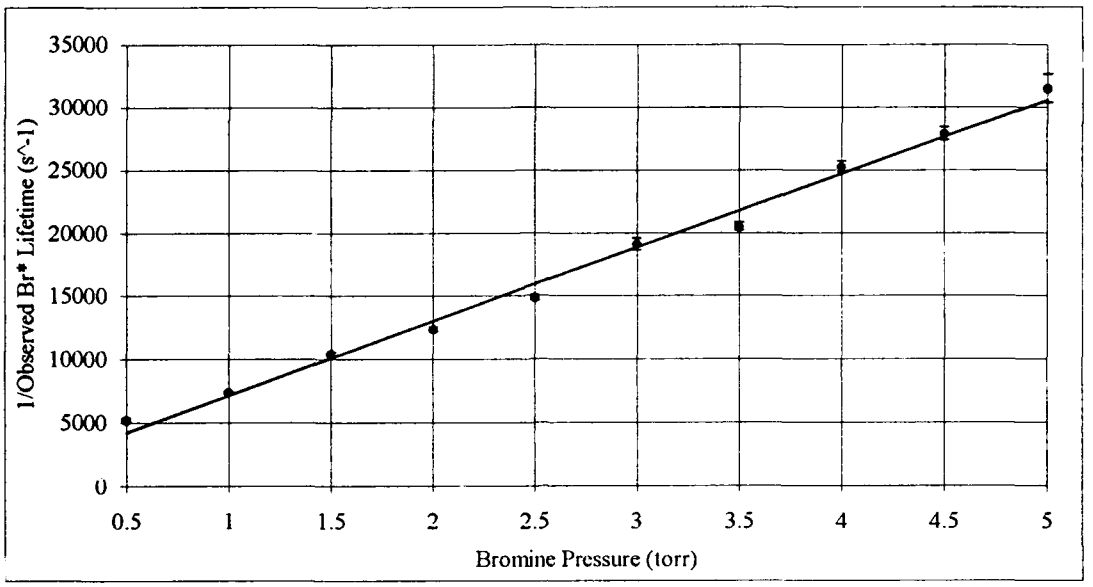

Figure 5.3 Stern - Volmer Analysis from Double Exponential Fit Data -- Decay Data

The r^2 fitting coefficient for this data is 0.9920. The equation which describes the linear fit in Figure 5.3 has the form

$$y = 1321.3333 + 5859.4061x \tag{5.4}$$

The rate coefficient is again derived by dividing the slope of the line by the number of bromine molecules per cm^3 per torr of gas:

$$k_1 = \frac{5859.4061}{3.22 \times 10^{16}} = 1.8197 \times 10^{-13} \frac{cm^3}{sec \cdot molecule} \tag{5.5}$$

This value is in rough agreement with the value obtain using the single exponential fit. Ramifications of these two values obtained will be discussed in the next chapter. In a similar manner a fit was attempted of the "c" coefficients. Figure 5.4 shows the results:

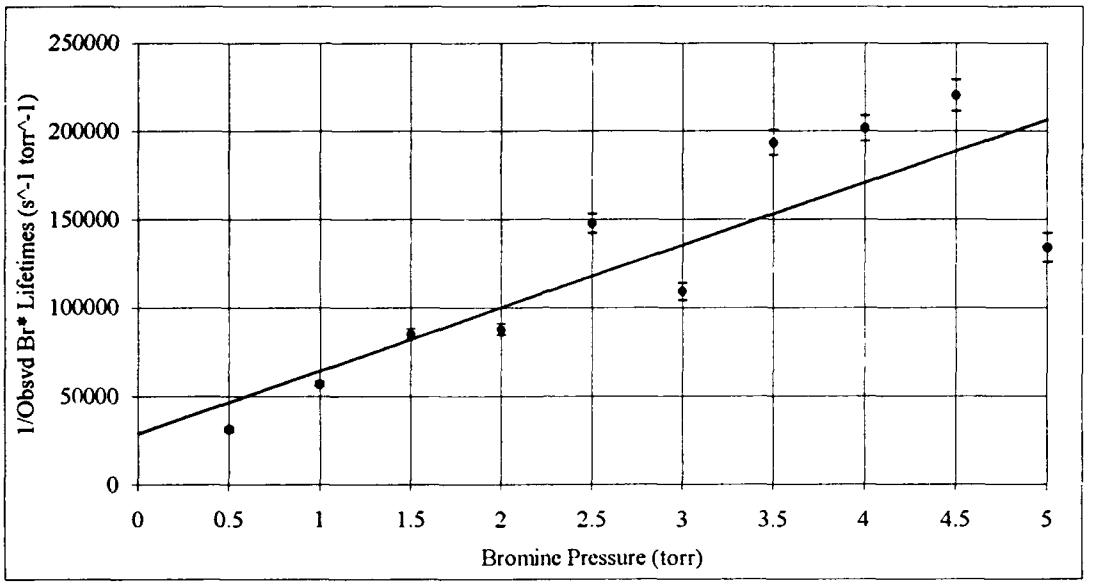

Figure 5.4 Stern - Volmer Analysis from Double Exponential Fit Data -- Rise Data

The r^2 fitting coefficient for this data is 0.7046. The term from (5.3) which contains the "c" coefficient represents an as yet undetermined rate process. The functional form which describes the linear fit in Figure 5.4:

$$y = 29146.933 + 35494.024x \tag{5.6}$$

This yields a rate of

$$k_2 = \frac{35494.024}{3.22 \times 10^{16}} = 1.1023 \times 10^{-12} \frac{cm^3}{sec \cdot molecule} \tag{5.7}$$

$CO_2^{\dagger}$ Fluorescence Data

Data representing the excited state of CO_2 ([101]), born via E ⇨ V transfer from Br*, is obtained in a similar manner. Figure 5.5 shows fluorescence signals obtain at a fixed Br_2 pressure, while varying the CO_2 pressure. Although the intensity scale is arbitrary, the relative scales on both the Br* and [101] data plots are equivalent. Note that the signal is nearly an order of magnitude greater than the Br* signal at 250 mtorr of CO_2. Clearly, the broadband filter is effective at detecting [101] emission.

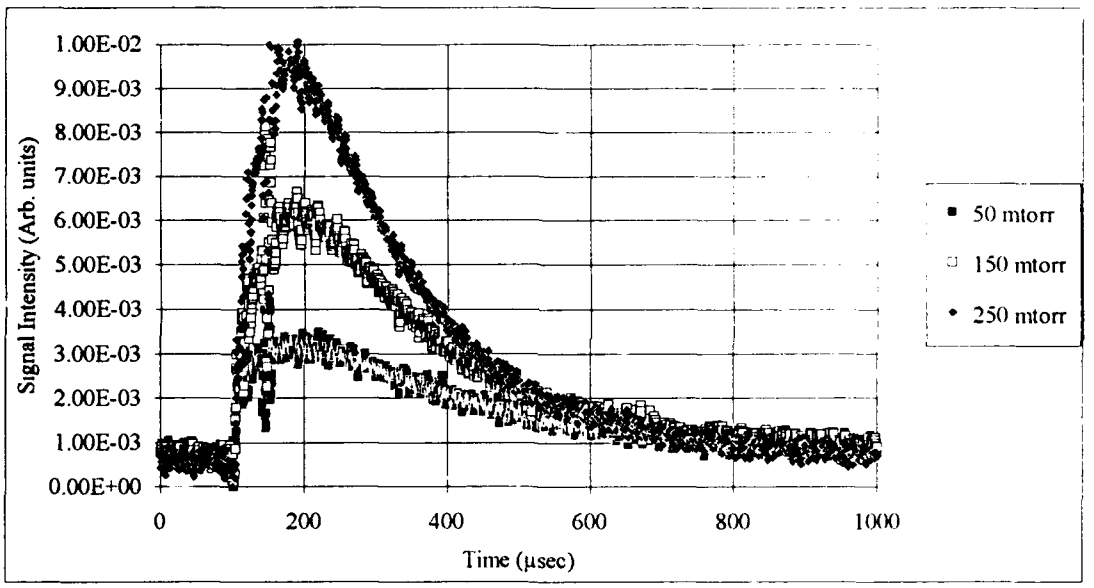

Figure 5.5 CO_2 Molecular Fluorescence Profiles

A series of data was taken at a fixed concentration of CO_2 (200 mtorr), while varying the bromine pressure. Again, an attempt to is made to fit the data to a generic double exponential function of the same form as (5.8):

$$y = a\left(e^{-bx} - e^{-cx}\right) \tag{5.9}$$

Table 5.3 shows the fit results obtained from TableCurve:

Br_2 Pressure	"b" coefficient	"c" coefficient	r^2 fit coefficient
0.5 torr	7323.58774	48400.6154	0.9579392083
1.0 torr	9636.57613	60361.9191	0.9736937793
1.5 torr	13435.6598	68044.0777	0.9803948714
2.0 torr	14948.4168	114906.831	0.9739028554
2.5 torr	16404.8477	156798.579	0.9498685721
3.0 torr	19638.6097	134272.578	0.9673591756
3.5 torr	19144.4656	151356.129	0.9555309331
4.0 torr	21834.235	148746.994	0.9589829832
4.5 torr	23859.7166	171376.643	0.9535046753
5.0 torr	25986.6952	178544.673	0.9368101858

Table 5.3 [101] Fluorescence Data Fit Parameters

We can arrive at an effective decay rate by again performing a Stern-Volmer analysis on the "b" coefficients calculated from the fitting process. Figure 5.6 shows the linear regression analysis performed on the data.

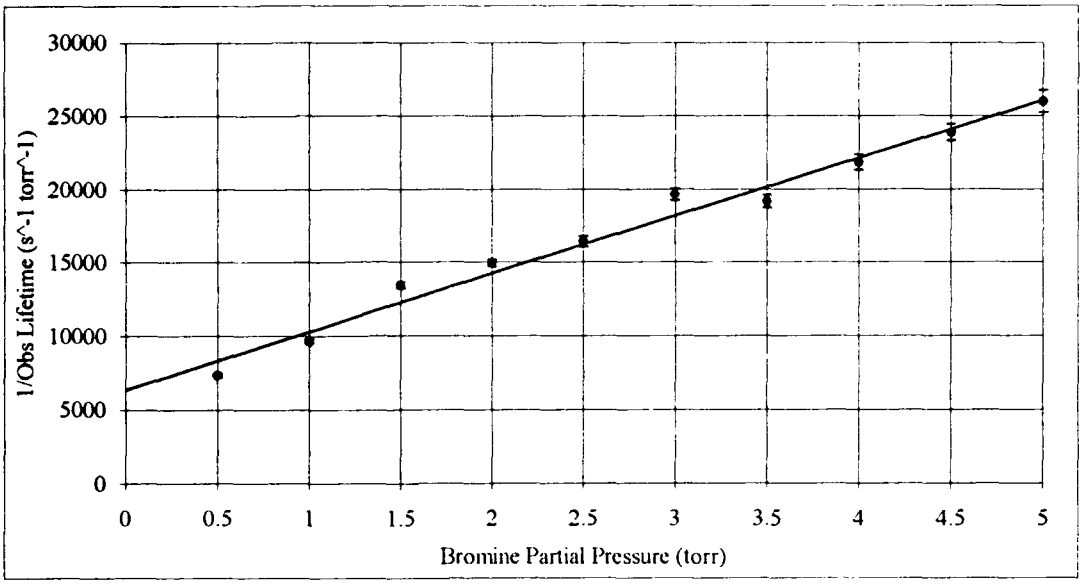

Figure 5.6 Stern - Volmer Decay Lifetime Rate Analysis -- From Molecular Fluorescence

A straight line fit to the "b" coefficients yields the line determined by the equation

$$y = 6376.3 + 3943.515x \tag{5.10}$$

The r^2 fitting coefficient here is 0.9798. Dividing the slope of (5.10) by the molar concentration of gas per torr yields

$$k_3 = \frac{3943.515}{3.22 \times 10^{16}} = 1.2247 \times 10^{-13} \frac{cm^3}{sec \cdot molecule} \tag{5.11}$$

Charting the rising exponential yields the following data:

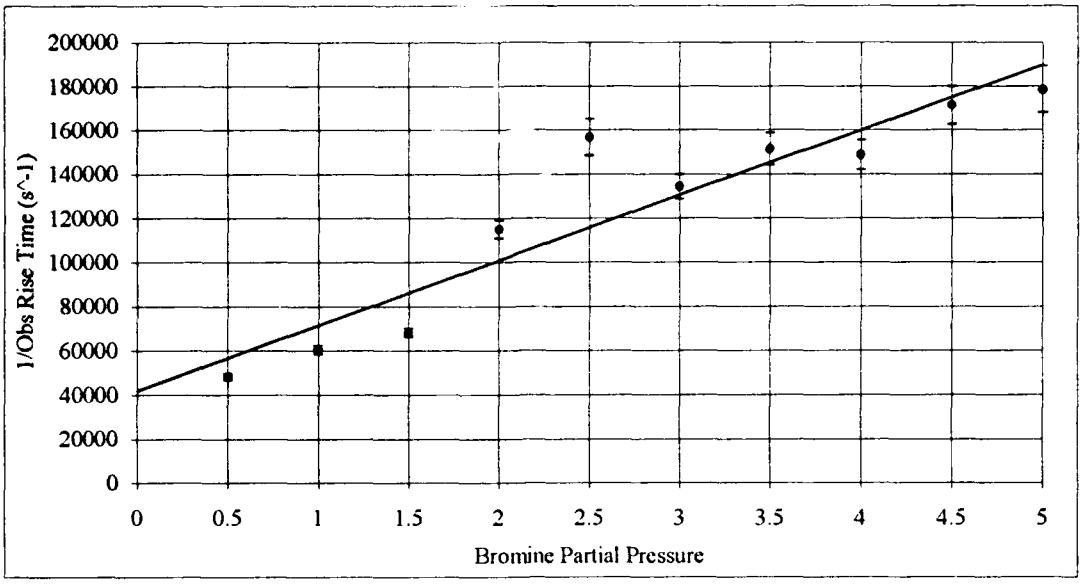

Figure 5.7 Stern - Volmer Rise Data Rate Analysis -- From Molecular Fluorescence

A straight line fit to the "c" coefficients yields the line determined by the equation

$$y = 41989.82 + 29560.45x \tag{5.12}$$

The r^2 fitting coefficient here is 0.8692. Dividing the slope of (5.12) by the molar concentration of gas per torr yields

$$k_4 = \frac{29560.45}{3.22 \times 10^{16}} = 9.1803 \times 10^{-13} \frac{cm^3}{sec \cdot molecule} \tag{5.13}$$

The final set of rate measurements is obtained by inserting a second interference filter in front of the InSb side-viewing detector, and varying the CO_2 concentration while keeping the Br_2 concentration fixed . This secondary filter has a much narrower bandwidth (FWHM ~ 0.02 μm), and is centered at 4.3 μm. The now familiar double exponential fitting process was applied to the data leading to the following table of values:

Br_2 Pressure	"b" coefficient	"c" coefficient	r^2 fit coefficient
1.0 torr	27442.6368	175997.548	0.9645840399
1.5 torr	30226.6055	170672.855	0.9697662945
2.0 torr	32148.7908	168664.635	0.9687853256
2.5 torr	34352.6718	166640.872	0.9699428838
3.0 torr	37170.4601	161542.05	0.9698193906
3.5 torr	38321.2059	164310.019	0.969547746
4.0 torr	39803.3743	165259.674	0.9681478628
4.5 torr	42011.4012	163629.006	0.9673162594
5.0 torr	43793.6416	163836.681	0.9642287559

Table 5.4 [101] Quenching Data Fit Parameters

Figure 5.8 shows the linear fit to the decay (b) coefficients:

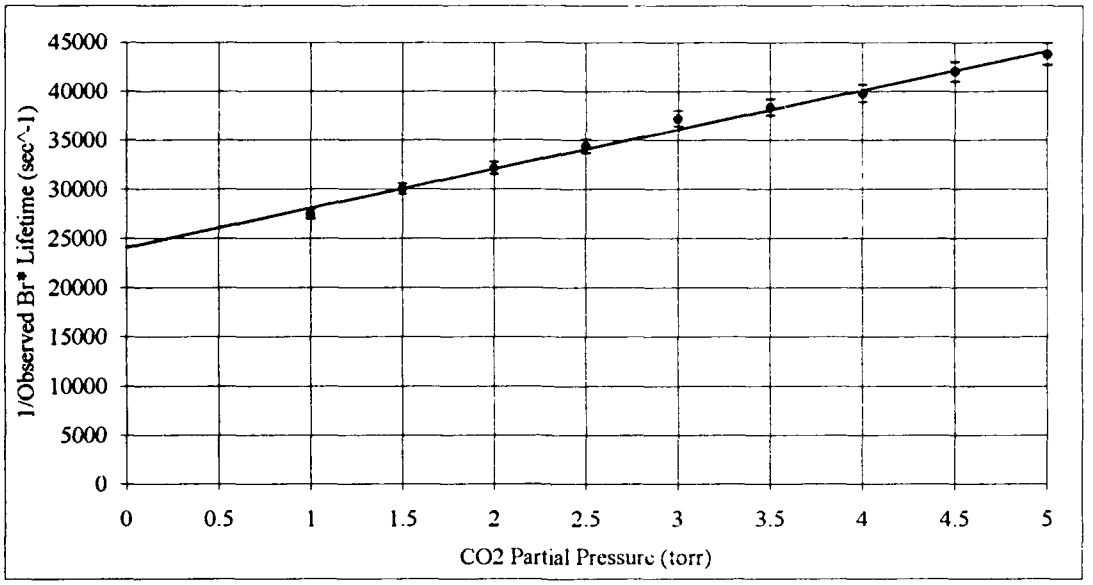

Figure 5.8 Stern-Volmer Analysis of Decay Data from 4.3 μm Fluorescence

A straight line fit yields the line determined by the equation

$$y = 24055.8 + 4021.067x \tag{5.14}$$

The r^2 fitting coefficient here is 0.9923. Dividing the slope of (5.14) by the molar concentration of gas per torr yields

$$k_5 = \frac{4021.067}{3.22 \times 10^{16}} = 1.2488 \times 10^{-13} \frac{cm^3}{sec \cdot molecule} \tag{5.15}$$

A look at the rise of the molecular fluorescence data as viewed through the 4.3 μm filter is less conclusive:

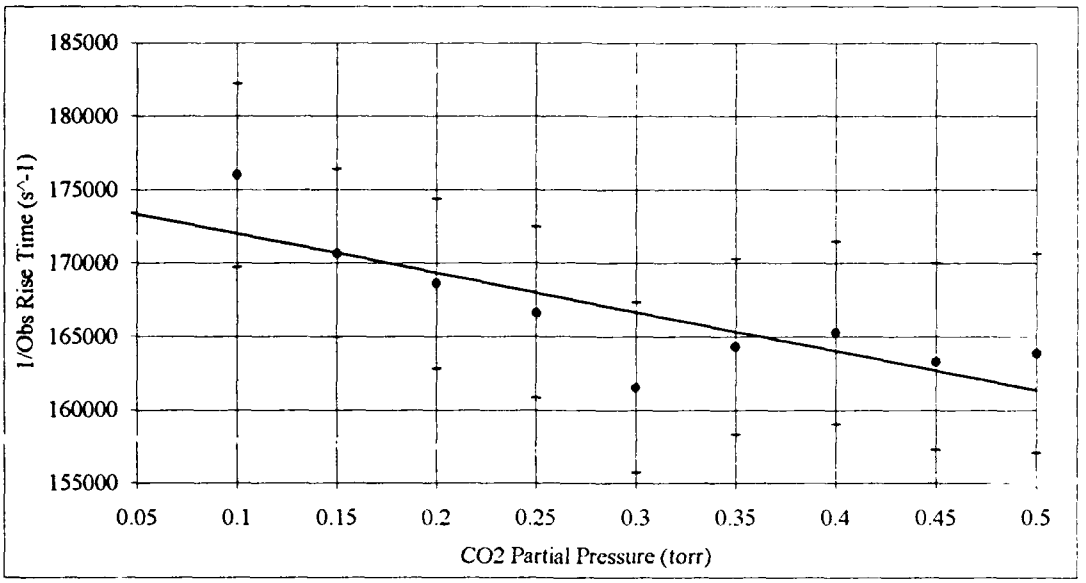

Figure 5.9 Stern-Volmer Analysis of Rise Data from 4.3 μm Fluorescence

A straight line fit yields the line determined by the equation

$$y = 174688 - 26665.7x \tag{5.16}$$

The r^2 fitting coefficient here is 0.6647. Dividing the slope of (5.16) by the molar concentration of gas per torr yields

$$k_6 = \frac{26665.7}{3.22 \times 10^{16}} = 8.2813 \times 10^{-13} \frac{cm^3}{sec \cdot molecule} \tag{5.17}$$

The negative slope observed obviously represents a non-physical result. The convolution of possible 4.3 μm transitions, combined with a simple double exponential model are likely the cause for this trend in the data.

Br - CO_2 Laser Demonstration Results*

In a word, the Br* - CO_2 E⇨V energy transfer laser demonstration was unsuccessful. Several attempts were made to achieve stimulated emission on both the 4.3 and 10.6 μm transitions. No signal was ever detected on the HgCdTe detector. Several different detectors were tried, as well as a number of output coupling schemes, but to no avail. It is believed that the pump energy was insufficient, despite having performed calculations to the contrary. The best available pump energy from our experimental setup

$$E_{pump} = \frac{\text{avg pump power}}{\text{pulse rep rate}} = \frac{62\text{mW}}{25\text{Hz}} = 2.48\text{mJ} \qquad (5.18)$$

could not, according to Pastel, support lasing. A minimum of 12 mJ was necessary to see stimulated emission using an experimental apparatus very similar to ours (8:569). Our calculations also assumed a best case scenario in terms of mirror reflectivities, cavity losses, etc.

VI. Discussion and Recommendations for Future Work

Introduction

This final section discusses the results achieved and possible interpretations for the rate data. Recommendations are offered for future efforts in this area.

Discussion

§ Quenching Rate Analysis

We summarize the quenching rates observed from this effort:

Measurement Conditions	**Rate Coefficient**	**Suspected Reaction**
Br_2 Sample Only Broadband 2.71 μm filter Single exponential fit	$k_{fall} = 1.65\times10^{-13}$ cm^3 mol^{-1} sec^{-1}	$Br_2 + Br^* \Rightarrow 3Br$ $CO_2(101) + CO_2(000) \Rightarrow$ $CO_2(100) + CO_2^*$
Br_2 Sample Only Broadband 2.71 μm filter Double exponential fit	$k_{fall} = 1.82\times10^{-13}$ cm^3 mol^{-1} sec^{-1} $k_{rise} = 1.10\times10^{-12}$ cm^3 mol^{-1} sec^{-1}	$Br_2 + Br^* \Rightarrow 3Br$ $CO_2(101) + CO_2(000) \Rightarrow$ $CO_2(100) + CO_2^*$
$Br_2 + CO_2$ Sample Broadband 2.71 μm filter Double exponential fit	$k_{fall} = 1.22\times10^{-13}$ cm^3 mol^{-1} sec^{-1} $k_{rise} = 9.18\times10^{-13}$ cm^3 mol^{-1} sec^{-1}	$Br^* + CO_2(000) \Rightarrow$ $Br + CO_2$ (all states) $CO_2(101) + CO_2(000) \Rightarrow$ $CO_2(100) + CO_2^*$
$Br_2 + CO_2$ Sample 4.3 μm + 2.71 μm filters Double exponential fit	$k_{fall} = 1.25\times10^{-13}$ cm^3 mol^{-1} sec^{-1} $k_{rise} = 8.28\times10^{-13}$ cm^3 mol^{-1} sec^{-1}	$Br^* + CO_2(000) \Rightarrow$ $Br + CO_2$ (all states) $CO_2(101) + CO_2(000) \Rightarrow$ $CO_2(100) + CO_2^*$

Table 6.1 Quenching Rate Coefficient Data

As a base for comparison, previously measured quenching rates are quoted:

Reaction	Quenching Rate Coefficient (10^{-12} cm^3 molecule^{-1} sec^{-1})	Rate Reference
$Br_2 + Br^* \Rightarrow 3Br$	0.48 ± 0.05 1.2 ± 0.3	(6:317) (2:1875)
$Br^* + CO_2(000) \Rightarrow$ $Br + CO_2$ (all states)	15 ± 1	(1:4458)
$CO_2(101) + CO_2(000) \Rightarrow$ $CO_2(100) + CO_2^*$	130	(8:569)
$Br^* + CO_2(000) \Rightarrow$ $Br + CO_2(101)$	5.6 ± 2.8 6.0	(10:306) (1:4460)

Table 6.2 Previously Observed Quenching Rate Coefficient Data

The average decay rate from the *Br_2 sample only* (from both single and double exponential fits $\Rightarrow 1.735 \times 10^{-13}$ cm^3 mol^{-1} sec^{-1}) is slower by factors of 2.8 and 6.9 from previous efforts. Accurately accounting for these differences has proven to be difficult due to the transmissivity of the broadband 2.71 μm interference filter. Figure 6.1 shows the transmission of this filter as function of wavelength:

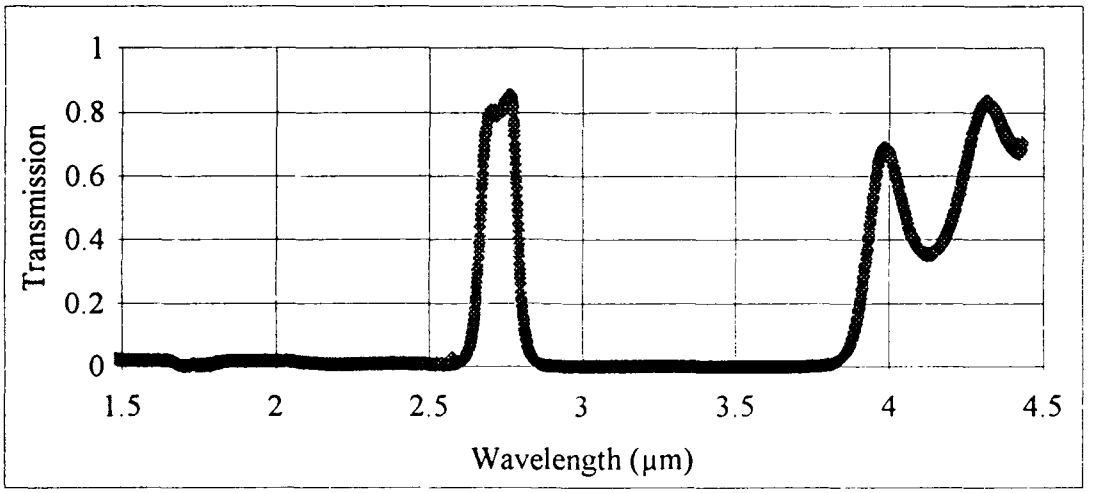

Figure 6.1 Transmission Characteristics of Broadband 2.71 μm Interference Filter

Note that there is significant radiation in the region of 4.3 μm that is passed by this filter. Molecular fluorescence from even small amounts (~ 1%) of CO_2 impurities in the system could be masking the much weaker Br* fluorescence. Determining a precise mechanism to account for the observed quenching is not possible, however, as there may be several vibrational transitions in the vicinity of 4.3 μm fluorescing. Deconvolving the various rate processes is beyond the scope of this effort.

The molecular fluorescence interference is further supported by observing the finite rise of the *Br_2 sample only* data. In the time frame of interest, the Br* is created nearly instantaneously. There should be no observable rise time of the Br* fluorescence. The rate that is observed here, $k_{rise} = 1.10\times10^{-12}$ cm^3 mol^{-1} sec^{-1}, may be the result of specifically CO_2 contamination. We know the [101] state of CO_2 to be the primary $E \leftrightarrows V$ energy transfer channel from Br* (11:1051). Deactivation of [101] by ground state CO_2 is fast--nearly gas kinetic, as shown in Table 6.2. If we assume a 1% contamination of the Br_2 sample by CO_2, we would have an effective quenching rate of

$$\{[000]+[101]\}\frac{[000]}{[Br_2]} = 1.3\times10^{-10}(0.01) = 1.3\times10^{-12}\frac{cm^3}{mol\cdot sec} \qquad (6.1)$$

which is within 20% of our observations. With such a small concentration of CO_2, we would expect the quenching rate to be degraded in such a fashion.

After adding CO_2 to the system, similar convoluting of rate processes appeared to be at work. In the first of the two Br_2 + CO_2 experiments (row 3 of Table 6.1), 200 mtorr of CO_2 was added to a fixed amount of Br_2; then the Br_2 concentration adjusted up to a total concentration of 5 torr of Br_2. We conditionally ascribe the rate of decay of the fluorescence to quenching of Br* by ground state CO_2:

$$Br^* + [000] \rightarrow Br + CO_2(\text{all states}) \qquad (6.2)$$

$$Br^* + [000] \xrightarrow{E \rightarrow V} Br + [101] \qquad (6.3)$$

where we have specifically identified the primary E⇨V pathway in (6.3). The poor out-of-band rejection of the broadband 2.71 μm filter is immediately evident by comparing the rates observed for this sample and the final data sample, where a 4.3 μm filter was placed in front of the broadband 2.71 μm filter. The rates observed in the two experiments are nearly identical, within the experimental error. This confirms our belief that the primary emission being observed is the [101] - [100] transition of CO_2. And since we are not isolating the Br* emission at 2.71 μm, establishing the quenching rate of CO_2 on Br* cannot be achieved. In fact, the observed decay is most likely the result of the deactivation of the [101] state by a variety of processes including V⇨V intramolecular energy transfer to lower vibrational states.

It should be clear that in order to extract quenching rates for Br*, complete isolation of the Br* fluorescence must be achieved. This is accomplished by using a narrow band filter (FWHM ≤ 0.01 μm) with complete out-of-band rejection. Experiments are currently in progress using an appropriate filter. Preliminary results are encouraging. Determining the reactions which would explain the rates observed for the Br_2 + CO_2 system requires a more sophisticated model for [101] relaxation. Future efforts to isolate specific vibrational transitions in CO_2 may prove fruitful.

§ Br - CO_2 Laser Feasibility Analysis*

As stated previously, efforts were unsuccessful to lase on the 4.3 μm ([101] - [100]) transition of CO_2. All signs point to insufficient pump photon energy. Measurements were made of scattering losses in the cavity to determine actual pump energies available to the gain medium. Figure 6.2 shows where average power measurements were made in the cavity:

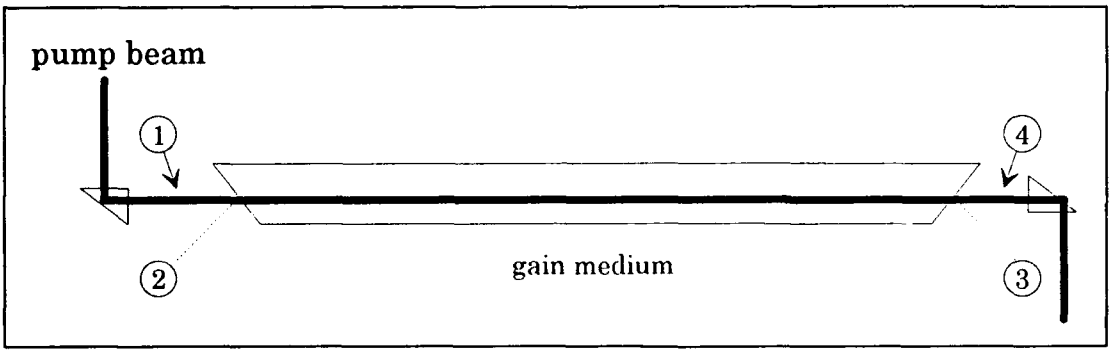

Figure 6.2 Cavity Scattering Loss Measurements

Average power measurements were made using the He-Ne alignment laser. Table 6.3 indicates our results:

Source Laser	Measurement Location	Average Power
He-Ne	1	430 μW
"	2	2.7 μW
"	3	1.1 μW
"	4	418 μW

Table 6.3 Cavity Scattering Measurements

The cavity scattering loss measurements made with the He-Ne laser would suggest that our assumption of a 1.5% pump beam scattering loss per gain medium brewster window is reasonable:

$$\frac{(430\mu W - 418\mu W)}{430\mu W} = 2.79\% \qquad (6.4)$$

There are several suggestions to achieve stimulated emission which should be considered. Switching the pump source seems the most obvious solution. A frequency-doubled Nd:YAG pulsed laser operating at 532 nm would provide the necessary pump energy (using IBr as a donor for Br*). The output coupling scheme could be improved as well. Output coupling using dielectric cavity mirrors would greatly simplify the task of positioning the HgCdTe detector, while not compromising (most likely improving) the output coupling fraction. Replacing the prisms as well with dielectric-coated mirrors would significantly improve the fraction of pump energy reaching the cavity.

Bibliography

1. Hariri, A. and C. Wittig. "Electronic to Vibrational Energy Transfer from Br($4^2P_{1/2}$) to CO_2, COS, and CS_2," *Journal of Chemical Physics,* 67:4454-4462 (November 1977).

2. Hariri, A. and C. Wittig. "Electronic-Vibrational Energy Transfer from Br($4^2P_{1/2}$) to HCN, and Deactivation of HCN(001)*," *Journal of Chemical Physics,* 65:1872-1875 (September 1976).

3. Haugen, Harold K., Eric Weitz, and Stephen R. Leone. "Accurate Quantum Yields by Laser Gain versus Absorption Spectroscopy: Investigation of Br/Br* Channels in Photofragmentation of Br_2 and IBr," *Journal of Chemical Physics,* 83:3402-3412 (October 1985).

4. Herzberg, Gerhard. *Molecular Spectra and Molecular Structure II. Infrared and Raman Spectra of Polyatomic Molecules.* New York: Van Nostrand Reinhold Company, 1945.

5. Johnson, Ray O. "Studies In Br($^2P_{1/2}$) Excited Atomic Bromine Energy Transfer and Quenching Mechanisms," *Dissertation Prospectus,* Air Force Institute of Technology, Wright-Patterson AFB, OH, March 1992.

6. Leone, Stephen R. and Francis J. Wodarczyk. "Laser-Excited Electronic-to-Vibrational Energy Transfer from Br($4^2P_{1/2}$) to HCl and HBr," *Journal of Chemical Physics,* 60:314 (January 1974).

7. Okabe, Hideo. *Photochemistry of Small Molecules.* New York : John Wiley and Sons, 1978.

8. Pastel, R. L. and others. "Efficient Br* Laser Pumped by Frequency-Doubled Nd:YAG and Electronic-to-Vibrational Transfer Pumped CO_2 and HCN Lasers," *Chemical Physics Letters,* 183:565-569 (September 1991).

9. Perram, Glen P. Professor, School of Engineering Physics, Personal Interviews. Air Force Institute of Technology, Wright-Patterson AFB, OH, July - September 1992.

10. Peterson, Alan B., Curt Wittig, and Stephen R. Leone. "Infrared Molecular Lasers Pumped by Electronic-Vibrational Energy Transfer from Br($4^2P_{1/2}$): CO_2, N_2O, HCN, and C_2H_2," *Applied Physics Letters,* 27:305-306 (September 1975).

11. Peterson, Alan B., Curt Wittig, and Stephen R. Leone. "Electronic-to-Vibrational Pumped CO_2 Laser Operating at 4.3, 10.6, and 14.1 μm," *Journal of Applied Physics,* 47:1051-1054 (March 1976).

12. Tate, Ralph F. "Steady-State Production and Quenching of $Br(^2P_{1/2})$," *Thesis*, Air Force Institute of Technology, Wright-Patterson AFB, OH, October 1991.

13. Verdeyen, Joseph T. *Laser Electronics*, Englewood Cliffs, NJ: Prentice Hall, 1989.

14. Weast, Robert C. *Handbook of Chemistry Physics (55th Edition)*, Cleveland, OH: CRC Press, 1974.

15. Witteman, W.J. *The CO_2 Laser*, Berlin: Springer-Verlag, 1987.

Vita

Captain Steven M. Katapski was born on 18 November 1959 in Virginia Beach, VA. He graduated from El Toro High School in El Toro, CA in 1977. In June of 1982 he graduated from the United States Air Force Academy with a Bachelor of Science degree in Atmospheric Physics, and was assigned to the Air Force Space Division at Los Angeles AFS, CA, where he worked as a project officer for the Advanced Space Technology Directorate. In May of 1986 he was reassigned to the Air Force Weapons Laboratory where he served as the deputy program manager for mission operations for the highly successful Relay Mirror Experiment, a Strategic Defense Initiative technology demonstration program to advance the state-of-the-art in laser pointing, tracking, and acquisition using both ground and space-based assets. He accepted an assignment to the School of Engineering, Air Force Institute of Technology, in May 1991.

Permanent Address: 23732 Cavanaugh Rd.
El Toro, CA

REPORT DOCUMENTATION PAGE

Form Approved
OMB No. 0704-0188

1. AGENCY USE ONLY (Leave blank)	2. REPORT DATE	3. REPORT TYPE AND DATES COVERED
	November 1992	Master's Thesis

4. TITLE AND SUBTITLE
Electronic-to-Vibrational Energy Transfer from Br* to CO_2 & Electronic-to-Vibrational Laser Feasibility Studies

5. FUNDING NUMBERS

6. AUTHOR(S)
Captain Steven M. Katapski

7. PERFORMING ORGANIZATION NAME(S) AND ADDRESS(ES)
Air Force Institute of Technology, WPAFB, OH 45433-6583

8. PERFORMING ORGANIZATION REPORT NUMBER
AFIT/GEP/ENP/92D-07

9. SPONSORING/MONITORING AGENCY NAME(S) AND ADDRESS(ES)
Dr Ernie Dorko
PL/LIDB
Kirtland AFB, NM 87117-6008

10. SPONSORING/MONITORING AGENCY REPORT NUMBER

11. SUPPLEMENTARY NOTES

12a. DISTRIBUTION/AVAILABILITY STATEMENT
Approved for public release; distribution unlimited

12b. DISTRIBUTION CODE

13. ABSTRACT *(Maximum 200 words)*

The energy transfer mechanism from photo-excited bromine atoms ($Br(^2P_{1/2})$) to CO_2 is investigated in a pulsed fluorescence experiment. An excimer-pumped pulsed dye laser operating at 480 nm is used to photolyze molecular bromine, resulting in the creation of on excited state bromine atom and one ground state bromine atom. The electronically-excited bromine atoms (referred to as Br*) collide with and excite vibrational modes in the ground electronic state of CO_2. Measurements are made of the Br* lifetimes and associated quenching processes, and the electronic-to-vibrational energy transfer rate from Br* to CO_2. The feasibility of subsequent stimulated emission from the CO_2 on the (101) $\rightarrow$ (000) (4.3 micron) transition is studied, and attempts are made to achieve lasing. Limitations of the experimental apparatus prevented achieving lasing on the 4.3 micron transition. Recommendations are made for improvements in the analysis and apparatus for further research.

14. SUBJECT TERMS
Bromine, Spin-orbit relaxation, Quenching, E-V energy transfer

15. NUMBER OF PAGES
54

16. PRICE CODE

17. SECURITY CLASSIFICATION OF REPORT	18. SECURITY CLASSIFICATION OF THIS PAGE	19. SECURITY CLASSIFICATION OF ABSTRACT	20. LIMITATION OF ABSTRACT
Unclassified	Unclassified	Unclassified	UL

GENERAL INSTRUCTIONS FOR COMPLETING SF 298

The Report Documentation Page (RDP) is used in announcing and cataloging reports. It is important that this information be consistent with the rest of the report, particularly the cover and title page. Instructions for filling in each block of the form follow. It is important to ***stay within the lines*** to meet ***optical scanning requirements***.

Block 1. Agency Use Only *(Leave blank)*.

Block 2. Report Date. Full publication date including day, month, and year, if available (e.g. 1 Jan 88). Must cite at least the year.

Block 3. Type of Report and Dates Covered. State whether report is interim, final, etc. If applicable, enter inclusive report dates (e.g. 10 Jun 87 - 30 Jun 88).

Block 4. Title and Subtitle. A title is taken from the part of the report that provides the most meaningful and complete information. When a report is prepared in more than one volume, repeat the primary title, add volume number, and include subtitle for the specific volume. On classified documents enter the title classification in parentheses.

Block 5. Funding Numbers. To include contract and grant numbers; may include program element number(s), project number(s), task number(s), and work unit number(s). Use the following labels:

C	- Contract	**PR**	- Project
G	- Grant	**TA**	- Task
PE	- Program Element	**WU**	- Work Unit Accession No.

Block 6. Author(s). Name(s) of person(s) responsible for writing the report, performing the research, or credited with the content of the report. If editor or compiler, this should follow the name(s).

Block 7. Performing Organization Name(s) and Address(es). Self-explanatory.

Block 8. Performing Organization Report Number. Enter the unique alphanumeric report number(s) assigned by the organization performing the report.

Block 9. Sponsoring/Monitoring Agency Name(s) and Address(es). Self-explanatory.

Block 10. Sponsoring/Monitoring Agency Report Number. *(If known)*

Block 11. Supplementary Notes. Enter information not included elsewhere such as: Prepared in cooperation with...; Trans. of...; To be published in.... When a report is revised, include a statement whether the new report supersedes or supplements the older report.

Block 12a. Distribution/Availability Statement. Denotes public availability or limitations. Cite any availability to the public. Enter additional limitations or special markings in all capitals (e.g. NOFORN, REL, ITAR).

- **DOD** - See DoDD 5230.24, "Distribution Statements on Technical Documents."
- **DOE** - See authorities.
- **NASA** - See Handbook NHB 2200.2.
- **NTIS** - Leave blank.

Block 12b. Distribution Code.

- **DOD** - Leave blank.
- **DOE** - Enter DOE distribution categories from the Standard Distribution for Unclassified Scientific and Technical Reports.
- **NASA** - Leave blank.
- **NTIS** - Leave blank.

Block 13. Abstract. Include a brief *(Maximum 200 words)* factual summary of the most significant information contained in the report.

Block 14. Subject Terms. Keywords or phrases identifying major subjects in the report.

Block 15. Number of Pages. Enter the total number of pages.

Block 16. Price Code. Enter appropriate price code *(NTIS only)*.

Blocks 17. - 19. Security Classifications. Self-explanatory. Enter U.S. Security Classification in accordance with U.S. Security Regulations (i.e., UNCLASSIFIED). If form contains classified information, stamp classification on the top and bottom of the page.

Block 20. Limitation of Abstract. This block must be completed to assign a limitation to the abstract. Enter either UL (unlimited) or SAR (same as report). An entry in this block is necessary if the abstract is to be limited. If blank, the abstract is assumed to be unlimited.